THERMAL PATTERNS OF SUBSURFACE FLOW REGIMES IN A MANTLED KARST AQUIFER NW ARKANSAS

Ryan T. Doucette

68 Pages May 2012

This thesis reports the results of a six month thermal investigation that monitored varying groundwater flow paths in a mantled karst aquifer.

THERMAL PATTERNS OF SUBSURFACE FLOW REGIMES IN A MANTLED KARST AQUIFER NW ARKANSAS

Ryan T. Doucette

68 Pages May 2012

A six month NW Arkansas thermal investigation utilized temperature and pressure loggers in 23 observation wells and six springs to monitor groundwater's thermal signal and stage height. Varying karst flow components were assigned to one of the three thermal classifications: ineffective heat exchange, mixed, or effective heat exchange. Ineffective heat exchange signals represent short groundwater residence time, strong response to precipitation events, and a temperature trend that mimics surface air temperatures. Effective heat exchange is assigned to flow with prolonged groundwater residence time, muted response to precipitation events, and a near-constant groundwater thermal signal. Mixed thermal signals represent groundwater flow that possesses characteristics of both ineffective and effective heat exchange. Project goals were multi-orientated: a) to assign a distinct thermal pattern to each monitored flow component and

b) to determine if the 2011 NW Arkansas 100-year flood impacted groundwater temperatures.

Application of thermographs and hydrographs produce distinct thermal patterns for various aquifer flow paths. The 11-17 °C temperature trend and high response to precipitation events allows for the designation of an ineffective heat exchange signal for epikarst springs and Copperhead spring. The near-constant 15.6 °C signal for deep aquifer flow represents strong effective heat exchange. Alluvium, shallow well (epikarst), and Langle spring are designated as a mixed thermal pattern due to their muted response to precipitation events and the 11-21 °C temperature trend.

Combined analysis of a 100-year flood event model and thermographs displaying groundwater signals may potentially confirm the connected nature between surface and subsurface processes. Correlating the flood's daily maximum extent and groundwater response to precipitation events reveals that both precipitation and the surface flood impact subsurface temperatures. Furthermore, monitoring surface air temperature, precipitation events, and groundwater temperature along various karst aquifer flow paths allows for the designation of thermal patterns for each subsurface flow regime.

THERMAL PATTERNS OF SUBSURFACE FLOW REGIMES IN A MANTLED KARST AQUIFER NW ARKANSAS

RYAN T. DOUCETTE

A Thesis Submitted in Partial
Fulfillment of the Requirements
For the Degree of

MASTER OF SCIENCE

Department of Geography-Geology

ILLINOIS STATE UNIVERSITY

2012

THERMAL PATTERNS OF SUBSURFACE FLOW REGIMES IN A MANTLED KARST AQUIFER NW ARKANSAS

RYAN T. DOUCETTE

THESIS APPROVED:

_____

Date Eric W. Peterson, Chair

_____

Date John Kostelnick

_____

Date Lisa Tranel

CONTENTS

TABLES

FIGURES

ACKNOWLEDGEMENTS

The two-year process to complete this thesis would not have been achieved if not for the aid and support provided by colleagues, friends, and family. First and foremost, I would like to express my gratitude to Dr. Eric W. Peterson for his field assistance, insightful revisions, patience, and mentorship. Appreciation for my other two committee members, Dr. John Kostelnick and Dr. Lisa Tranel, is also acknowledged. Their expertise in ArcMap/ArcScene greatly advanced the visualization and modeling aspects of my thesis. For granting access to the Savoy Experimental Watershed research site I credit the collaborative nature of both Dr. Van Brahana and the University of Arkansas.

This thesis is dedicated to my parents: my mother for her never-ending encouragement and general interest throughout the process, and my father for instilling a methodical hard-working mentality. To you both, and others who explore this investigation, enjoy the wonders of hydrogeology.

R.T.D.

CHAPTER I

INTRODUCTION

1.1 Purpose, Significance, and Justification

Karst aquifers account for approximately 25% of the United States groundwater reserve (US EPA 1988). Creation of a karst aquifer occurs through the process of CO_2-bearing rainwater (pH ~5.5) dissolving soluble limestone (Brahana 1997). Dissolution of limestone produces an unknown and complex subsurface geometry that is delineated by hydrogeologists through the use of tracers. Comprehending the variety of subsurface flow regimes in a karst aquifer is represented with a triple permeability model (Figure 1) (White 2005). The triple permeability model categorizes groundwater movement into three specific flow paths: matrix, fractured epikarst, and conduit.

According to White (2005), subsurface flow via matrix in carbonate bedrock is not intrinsically different than other bedrock matrix flow. Logically, White (2005) applies Darcy's Law and enforces the concept that all laminar/tortuous matrix flow is similar despite any lithological differences. The nature of diffuse flow in the matrix causes groundwater to remain in the system for long periods of time. High storage and low transport rates within matrix flow allow groundwater to equilibrate with the bedrock temperature, thus producing an effective heat exchange thermal signature (Luhmann et al. 2011).

Note that the phrase *effective heat exchange* refers to the process of groundwater temperature reaching equilibrium with bedrock temperature due to long groundwater residence time. Alternatively, the phrase *ineffective heat exchange* refers to the process where groundwater temperatures are unable to reach thermal equilibrium with bedrock temperatures due to short groundwater residence time.

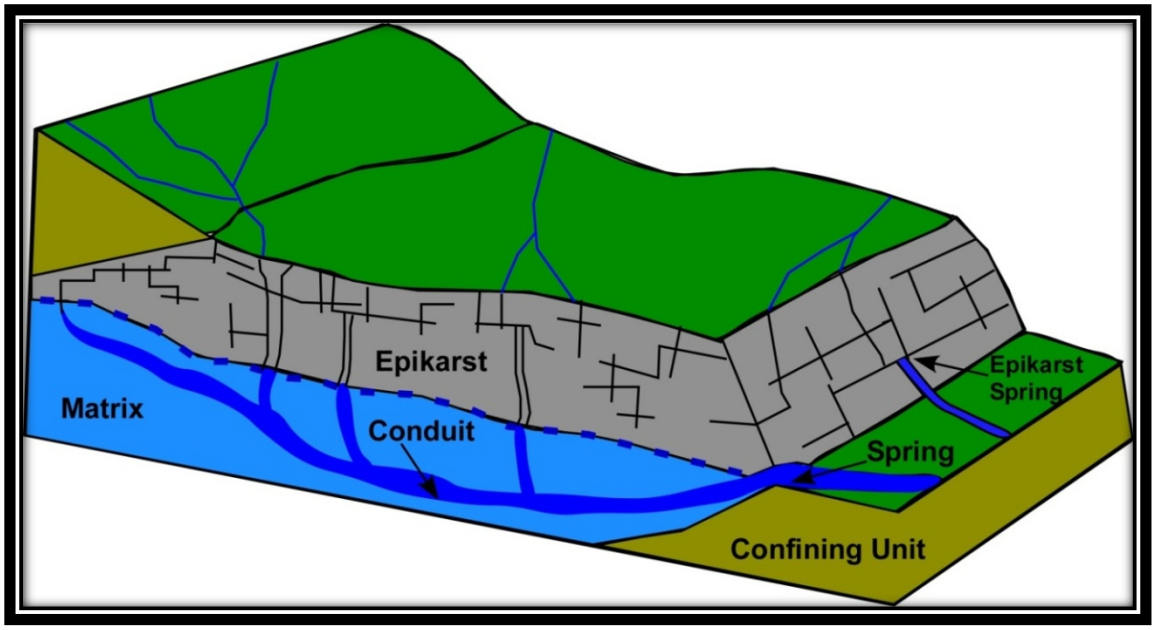

Figure 1: Block diagram of a heterogeneous anisotropic karst aquifer portraying zones of matrix, epikarst and conduits (modified from Goldscheider and Drew 2007).

In karst nomenclature, epikarst has numerous definitions. Krothe (2003) defines epikarst as the uppermost portion of the carbonate bedrock within the unsaturated zone, while Jones (2004) describes epikarst as a heterogeneous system between unconsolidated material and karstic rock that is partially saturated with water. Acidic soil waters dissolve carbonate bedrock to varying degrees, producing the *epikarst*, to be either systems of

high storage (e.g. perched aquifers), high transport (e.g. directly transferring recharge waters to groundwater), or a degree of both (Krothe 2003). Significance of epikarst flow is found in its capability to delay, store, or even re-route vertical infiltration towards the underlying aquifer. As for storing water, certain epikarst zones can be classified as reservoirs or aquifers.

Four maturity levels for epikarst zones are displayed in Figure 2. Characteristics of a *freshly exposed epikarst* zone include minimal fractures, low transport, and a high storage component. A *young epikarst* has prolonged periods of weathering, ultimately increasing the distribution, length, and width of fractures. Young epikarst units serve as low transport and high storage systems. A *mature soil covered* epikarst has a soil cover component that delays surface water infiltration. However, once flow reaches the mature epikarst zone, the high secondary porosity component vertically transfers the infiltrating waters into the underlying aquifer. Directly connected to the atmosphere, the *mature barren* epikarst represents a highly dissolved upper-layer of the carbonate bedrock. Surface waters infiltrating into the subsurface directly feed into the conduit network and are flushed to the underlying aquifer. To summarize, depending on level of maturity, epikarst may represent several thermal signatures. Long groundwater residence time (e.g. freshly exposed epikarst) would be indicative of effective heat exchange while short groundwater residence time (e.g. mature barren epikarst) would be indicative of ineffective heat exchange.

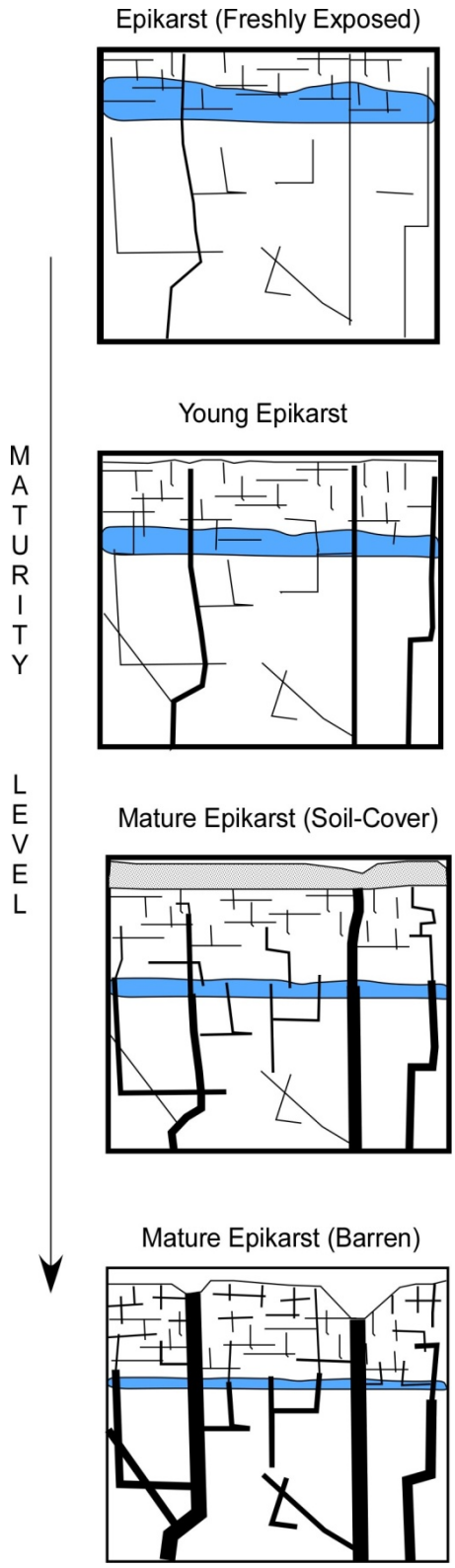

Figure 2: Diagram represents epikarst maturity level vs. exposure time (modified from Klimchouk, 2004).

Conduit dominant systems exhibit low storage and high transport rates (White 1999). Continued dissolution of carbonate bedrock produces enlarged fractures, potentially creating an environment where groundwater discharge may increase. The enlarged fractures, representative of conduit flow, produce a turbulent flow component. Conceptualize laminar *matrix* flow as driving gravel roads while turbulent *conduit tubes* would be equivalent to driving highways. Conduit routes shorten groundwater residence time. Therefore, short residence time inhibits equilibration between groundwater and bedrock temperature, producing an ineffective heat exchange signature (Luhmann et al. 2011).

Individual flow paths and their accompanying characteristics that produce turbulent and laminar flow are important in designating unique thermal signatures. Groundwater temperature signals are primarily derived from the effective and ineffective heat transport mechanism. In most cases, slow laminar flow allows groundwater to equilibrate with bedrock temperature whereas fast turbulent flow flushes through the system before thermal equilibration is achieved.

In certain karst aquifers, determining if the system is dominated by laminar or turbulent flow may be the key investigation; however, White (1999) reinstates the importance that basin relief is the overriding influence of water movement in the subsurface. White (1999) discusses how the head difference between high elevation points of recharge and low elevation points of discharge (i.e. springs) is the primary driving force of groundwater in the subsurface. For example, conduits are capable of transferring high volumes of water throughout an aquifer in locations with relatively high relief. However, in locations of gentle relief, the hydraulic gradient parameter is

insignificant and the driving force to flush water through the open pipe structures is diminished.

Determination of which flow component (matrix or conduit) is dominant coupled with understanding the role of epikarst to the overall aquifer system is unraveled through the use of tracers, data loggers, and modeling techniques (Yuan et al. 2008). In terms of tracers, thermal signals provide useful information when characterizing flow paths. Thermal investigations explore temperature to define varying groundwater flow paths from input to discharge locations. Monitoring heat transport at varying aquifer locations while also observing spring response to precipitation events allows researchers to determine recharge mode and system geometry of a karst aquifer (Luhmann et al. 2011).

A wide variety of karst studies have previously been conducted to determine if spring discharge water is characteristics of the overall karst system (Bonacci 1993), to assess the application of airborne thermography (Campbell et al. 1996), and to investigate thermal variations in the hyporheic zone of a karst stream (Dogwiler and Wicks 2006). Of particular interest for this investigation, Bonnacci (1993) focused on understanding spring hydrographs. Karst features (e.g. sink holes and sinking streams) produce a terrain where surface waters are scarce. Since the majority of surface water directly feeds to groundwater discharge locations, Bonnacci (1993) concluded that spring hydrographs are a proper method for capturing the overall karst aquifer system (e.g. storage rates, transportation rates, or even response to recharge events). In regards to spring hydrographs and other tracer methods (dye, isotope, and chemical), thermal tracers have been less explored. Advancing thermal tracer studies, Luhmann et al. (2011) applied

thermal tracers to cavern and spring flow with intention to monitor the primary input and output locations.

Luhmann et al. (2011) installed thermal loggers at four springs and two cave streams in SE Minnesota. Extracting the yearlong data from the thermal loggers, investigators produced thermographs detailing both surface/subsurface temperature signals and precipitation levels. Hydrographs were constructed to display the relationship between groundwater temperature and water level at cave and spring locations. Further, thermographs were utilized to display the degree of lag and amplitude of each individual temperature signal in response to air temperature and precipitation events while hydrographs depict the rate of flow (discharge) in relation to time. Spring measurements portray the overall responses of the aquifer to recharge events (Padilla et al. 1994). Generally, infiltration directly into quickflow pathways (conduits) produces greater spring responses. In contrast, infiltration directed into diffuse flow (matrix) has a limited/delayed impact on spring response. Analyzing thermal data in thermograph and hydrograph format is a useful and accurate way to assign thermal patterns for various groundwater flow paths. Overall, Luhmann et al. (2011) thermographs and hydrographs were utilized to delineate four distinct thermal patterns (Figure 3). The authors assigned each monitored flow path into one of the following four categories:

1. Ineffective heat exchange: Event Scale Variability (Pattern 1)
2. Ineffective heat exchange: Seasonal Variability (Pattern 2)
3. Effective heat exchange: Changing Aquifer Temperature (Pattern 3)
4. Effective heat exchange: Constant Aquifer Temperature (Pattern 4)

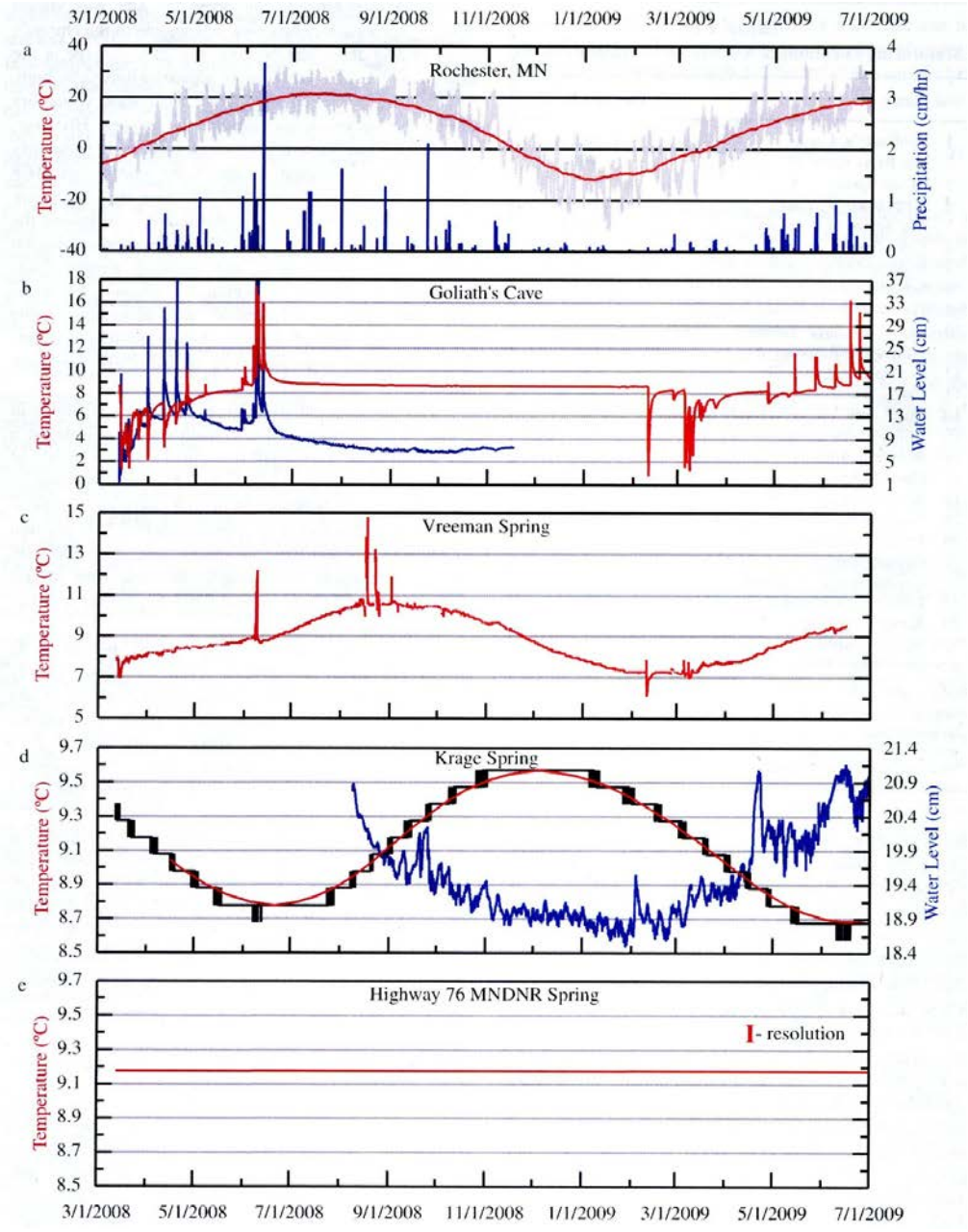

Figure 3: Thermograph and hydrograph compilations of particular thermal patterns in SE Minnesota. Colors within the graph correspond to the labeled y-axis colors. (a) The subdued gray line represents the hourly surface air temperature while overlaid by the two month running average red line. Also in (a) is the annual precipitation bar graph (b) temperature and water level of a stream which runs through a cavern (c) temperature at a spring representing event-scale variability and seasonal variability (d) temperature and water level at a spring which slightly varies in temperature in response to the changing aquifer temperature and (e) constant temperature from discharge from a constant temperature aquifer (Pattern 4). Note temperature and water level variations in Y-axis scales (Luhmann et al., 2011; Reprinted from *Ground Water* with permission of the National Ground Water Association. Copyright 2011).

Event-Scale Variability (Pattern 1): Event-scale variability (Figure 3b) represents recharge events where large volumes of water, originated by storm events or snow melt, flow through highly permeable fractures and conduit pathways (Luhmann et al. 2011). Dogwiler and Wicks (2006) explain that high hydrologic input into the system via quick flow pathways flush water through the system too quickly or in too great a volume to thermally equilibrate with the bedrock temperature. Quickflow groundwater exhibits ineffective heat exchange, typical of waters that flush through the system before equilibrium is reached. High rainfall or snow events are used by Luhmann et al. (2011) to illustrate event-scale variability within the aquifer system. Thermograph portrayal details the spike of groundwater temperature in response to the corresponding pulse of recharging waters. During colder months, the lower temperature surface waters impact groundwater temperatures and produce a negative change or drop in temperature. During warmer periods, the warm surface waters recharge the system and groundwater responds with a positive temperature spike.

Seasonal Variability (Pattern 2): Seasonal variability (Figure 3c) represents recharge waters that retain annual air temperature signals throughout the input to discharge groundwater transfer (Luhmann et al. 2011). In order for annual air temperatures to be mimicked by groundwater temperatures, a constant supply of recharge must be available. A direct surface stream input, specifically known as sinking streams, are karst features that provide a constant supply of recharge. Seasonal variability depicts an ineffective heat exchange. Springs with ineffective heat exchange, such as Figure 3 (c), display the following three conditions: (1) water temperatures that mimic surface air

temperature trends, (2) a degree of lag, and (3) positive or negative groundwater spikes in response to strong storm pulses.

Changing Aquifer Temperature (Pattern 3): Changing aquifer temperature (Figure 3d) represents effective heat exchange. Effective heat exchange is associated with long groundwater residence times. Prolonging groundwater residence time allows input water to equilibrate with bedrock temperatures. Dogwiler and Wicks (2006) explain thermal equilibrium between input waters and bedrock occurs through conductive and advective processes. Springs with effective heat exchange (Figure 3d) have groundwater discharge temperatures that annually vary between ~1-2 °C (Luhmann et al. 2011). Changing aquifer temperature lacks full equilibration and a constant discharge temperature primarily due to seasonal temperature fluctuation that influence near-surface bedrock temperature.

Constant Aquifer Temperature (Pattern 4): Constant aquifer temperature (Figure 3e) represents matrix flow. Laminar flow through the matrix is often times slow. Slow water movement is characteristic of an effective heat exchange flow path. In environments where constant bedrock temperatures are present, Dogwiler and Wicks (2006) state that long groundwater residence time (indifferent of matrix or conduit flow) will fully equilibrate to an ambient temperature that is in a direct reflection of mean annual temperature. In other words, springs representative of effective heat exchange indicate slow groundwater flow equilibrating with constant bedrock temperatures (Luhmann et al. 2011). Groundwater equilibrium with bedrock temperature is commonly exemplified by annual readings of < 1 °C temperature variance (Luhmann et al. 2011).

Clarification between effective heat exchange signatures (a) changing aquifer temperature and (b) constant aquifer temperature is required. Groundwater thermal signals representative of changing aquifer temperatures have a near-surface bedrock temperature that changes in correspondence to varying seasonal temperatures. However, the changing aquifer thermal signal lacks the degree of fluctuation/variation as exhibited by the ineffective heat exchange seasonal variability signature. Constant aquifer thermal signal is unaffected by fluctuating seasonal temperatures and maintains annual near-constant thermal signal.

Luhmann et al. (2011) summarize the thermographs and hydrographs with the Figure 4 flow chart. Authors subdivide the flow chart into ineffective and effective heat exchange routes. Further subdividing is represented by listing common parameters to each individual thermal signature, producing four distinct thermal patterns. Luhmann et al. (2011) acknowledge that alternative thermal patterns may result at different geographic locations.

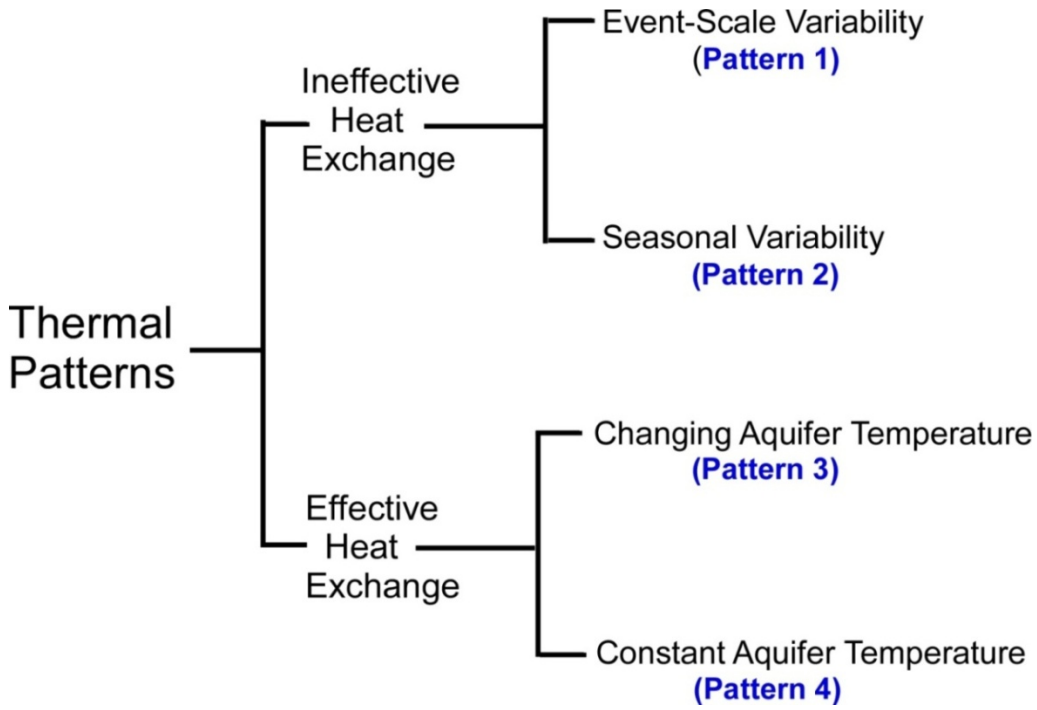

Figure 4: Flow chart delineating the four thermal patterns derived from ineffective and effective heat exchange in karst groundwater flow as proposed by Luhmann et al. (2011).

Karst aquifers contain both ineffective and effective flow paths, but the thermal signature derived at the drainage locations is indicative of the fraction of flow through thermally ineffective pathways (Luhmann et al. 2011). When conducting research within a karst terrain, one must determine the physical extent of the watershed as well as whether the focus of the investigation is on the local or regional scale. Infiltration of localized recharge directly enters the conduit/fracture network, producing an ineffective heat transport signature. Alternatively, an effective heat exchange thermal signal is commonly portrayed when recharge is viewed on the regional scale. Infiltration and flow through soil, rock matrix, and narrow aperture fractures before entering the main conduit/fracture network prolongs residence time and enhances equilibration (Luhmann

et al. 2011). Therefore, determining the fraction of localized vs. regional recharge is significant when designating karst thermal signatures.

Tracing temperature in solely cavern and spring locations may limit the ability to produce distinct thermal signatures along the flow network of a karst aquifer. Alternative investigation techniques were designed to monitor groundwater temperature at a variety of flow locations in order to accumulate data for the entire system. In summary, new collection methods trace subsurface flow paths throughout the entire groundwater system while previous thermal studies investigated strictly input and output locations.

Moreover, thermal tracers have been identified as being an accurate, cost-efficient, and non-labor intensive method for monitoring the subsurface. These characteristics are ideal when attempting to unravel the complex karst aquifer system. As White (2005) notes, varying storage and transport potential within separate flow paths produce a complex anisotropic heterogeneous system. In order to assign thermal signals to this system, new investigative techniques of installing thermal loggers throughout the entire flow system (e.g. input, output, and flow between these two locations via observation wells) have been incorporated. Overall, the purpose of the investigation was to install, monitor, and capture groundwater temperature signals throughout varying aquifer flow in order to designate distinct thermal patterns for each flow component.

Statement(s) of Investigation

1) Do different flow components in the NW Arkansas karst aquifer (e.g. alluvium, epikarst, epikarst springs, matrix, and springs) have distinct thermal signatures?
2) Does the 2011 NW Arkansas 100-year flood event impact groundwater's thermal signal?

1.2 Research Site

Located in northwest (NW) Arkansas (Figure 5), the research site is contained within a portion of the 1250 hectares of the Savoy Experimental Watershed (SEW). Owned by the University of Arkansas, the property resides ~16 kilometers (km) northwest of campus and is bounded on the west by the Illinois River. The University of Arkansas has collaborated with the United States Geological Survey (USGS) in an attempt to better understand karst terrains. Sharing of resources led to the installation of a vast number of hand augured shallow wells, air rotary drilled deep wells, and weirs to monitor groundwater quality and flow. Shallow wells range in depths of 4-10 (m) while deep wells were drilled to depths of 30-200 (m). Springs were monitored to determine the groundwater quality for the overall aquifer system. Furthermore, scientific collaboration of the USGS, faculty research, and graduate research has provided a strong foundation for groundwater processes occurring within the SEW mantled karst aquifer region. Specifically, a variety of tracer tests have been conducted and groundwater variables (i.e. flow paths, flow velocity, and modeling of cavern systems) are well documented (Brahana 1997).

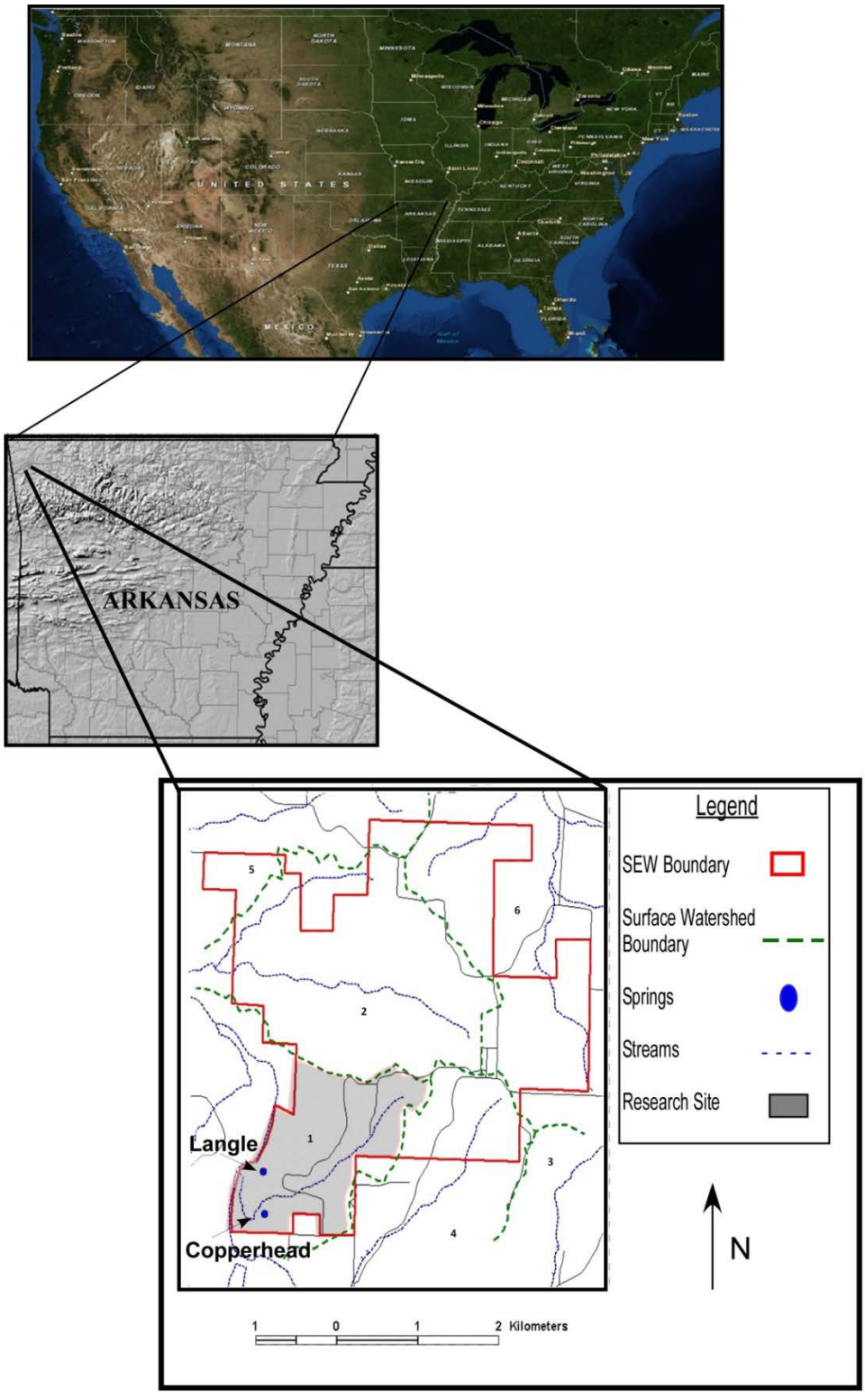

Figure 5: Within the United States, the research site is located in NW Arkansas (USGS 2010). Enlarged further, thermal equipment monitored SEW Basin 1 (modified from Brahana 1997).

1.3 Physiography

The SEW is located along the west-southwest flank of Ozark Highlands, where lands are dominated by steep ridges and shallow sinking valleys (Brahana 1997). The Ozark Highlands is also referred to the *Ozark Dome* due to the structural dome which underlays the region. Approximately 64,000 km^2 of area extends the Ozark Highlands into four states: Arkansas, Kansas, Missouri, and Oklahoma (Adamski et al. 1995).

1.4 Geology

Regionally, the Ozark Highlands are diverse in lithology, including a variety of igneous and sedimentary rocks (Adamski et al. 1995). The core of the igneous intrusion, which created the structural dome, is composed of a pre-Cambrian granitic composition; however, Paleozoic age sedimentary rocks flank the outer edges of the dome (Adamski et al. 1995). Structurally, Paleozoic rocks that were deposited on top of the igneous rocks of the Ozark dome display a slight southern dip of $< 1^{o}$ away from the dome's center (Phelan 2002). Structures of interest within the Ozarks are the Salem and Springfield Plateaus. Terrain of the Salem Plateau is generally characterized by the abundance of rolling hills, sinkholes, and springs (Adamski et al. 1995). While the Salem Plateau is underlain by Cambrian and Ordovician age geologic units, the Springfield Plateau overlays Mississippian-aged carbonate units. Although not as abundant as the Salem Plateau, sinkholes and springs are commonly exposed in the Springfield Plateau (Adamski et al. 1995).

Within the Springfield Plateau, the stratigraphy and composition of two geologic units are of particular importance: the Boone Formation and the St. Joe Member. In terms of lithology, the Boone Formation is described as a cherty limestone, where the chert serves as a confining unit (Brahana 1997). Sauer (2005) describes the Boone Formation's thin cherty limestone unit as being mantled. The term *mantled* is in reference to a soil/regolith residual weathering component that blankets the limestone bedrock. Fragment size within the soil/regolith tends to vary from fine to coarse. One of the two processes account for the stony soil covering: weathering of cherty limestone or alluvial deposition (Brahana 1997). Below the mantled layer, the upper zone of the cherty limestone unit, referred to as the epikarst, is determined to have a maturity level between the young → mature (soil cover) (Figure 2).

The St. Joe Formation, a Mississippian aged limestone, underlies the Boone Formation. Due to the crystalline-pure limestone composition, the St. Joe Formation karst features are further developed in magnitude and dimensions (Pennington 2010). Stratigraphic placement of the Boone Formation and the St. Joe Formation is important because primary basin discharge springs exist where the two contact one another. Overall, the stratigraphic column (Figure 6) details the aquifer bearing Mississippian age carbonate sequence as well as the underlying confining Devonian age shale unit (Phelan 2002).

1.5 Hydrogeology

Regionally, the Springfield Plateau aquifer consists of a Mississippian aged limestone and cherty limestone package, the Boone Formation (Adamski et al. 1995). When overlapping with the Springfield Plateau, the aquifer unit is unconfined. In unconfined regions, the aquifer is consistently recharged by precipitation events (Adamski et al. 1995). Structurally, the near horizontal beds have limited impact on surface/subsurface flow; however, Brahana (1997) states that faults and major joints exhibit strong structural control on groundwater flow. Another control on groundwater flow is the relative high secondary porosity, produced by prolonged dissolution and fracturing. Horizontal hydraulic conductivity is estimated as an order of magnitude greater than the vertical hydraulic conductivity (Adamski et al. 1995).

Locally, the Springfield Plateau aquifer is covered by a thin layer of rocky soil, regolith, and insoluble chert clasts (Brahana et al. 1997). Underneath the mantled portion is the Boone Formation, an impure cherty limestone geologic unit. The Boone Formation displays zones of karst formations; however, the underlying pure limestone St. Joe Member of the Boone Formation is the primary unit in which numerous springs, seeps, and caves occur (Brahana et al. 1997).

Underlying the SEW investigation site, complex subsurface geometry of the Springfield Plateau aquifer spans six surface water basins (Figure 5). Brahana et al. (1997) state that the varying flow paths throughout the six basins exhibit fast flowing groundwater. Tracing flow paths is difficult due to two primary reasons: a) complex subsurface geometry and b) the incongruent relationship between surface watersheds and groundwater watersheds. Ideally, surface watersheds and groundwater basins would

directly overlap. However, the varying watersheds within SEW tend to share subsurface connections, allowing for surface waters in one watershed to discharge from a separate groundwater watershed (Brahana 1997).

The incongruent relationship between surface watersheds and groundwater watersheds was explored by Brahana et al. (1998) with a dye trace study. Of interest, Brahana et al. (1998) investigated the two primary springs, Copperhead and Langle, in SEW Basin 1 (Figure 5). Copperhead spring, during periods with high precipitation levels and fast flow rates received a majority of the fluorescein dye. However, dry periods and slow groundwater flow was traced to Langle spring (Brahana et al. 1998). Independent of flow rates, westward flowing groundwater discharged into the nearby Illinois River.

Pennington (2010) supports and expands upon the discussions of both Al-Qinna (2003) and Brahana (1998) on the interrelated connectedness of Copperhead and Langle springs while referring to two conceptual models (reference Brahana et al.; 2005 Figures 9 & 10). Pennginton (2010) states that the two spring locations share a subsurface storage area. Described as a subsurface dam, ponded waters are restricted horizontal flow, producing vertical flow (Ting 2005). Conceptually, the vertically flowing water approaches the elevation at which the interconnected Copperhead and Langle basin (via bedding plane, enlarged fracture, or conduit flow) exist (Pennington 2010). According to Al-Rashidy (1999), Copperhead Spring resides at a slightly higher elevation than Langle Spring. Therefore, as long as the vertical flowing water and/or water table reside above the interconnected location, Langle Spring basin will overflow into the Copperhead basin. If a dry period occurs, the water table lowers below the interconnected elevation, Copperhead Spring returns to low-flow conditions, and Langle primarily receives the

bulk of the subsurface groundwater storage (Pennington 2010). During low flow states, Langle spring has been recorded as discharging twice the amount of water as Copperhead (Ting 2005).

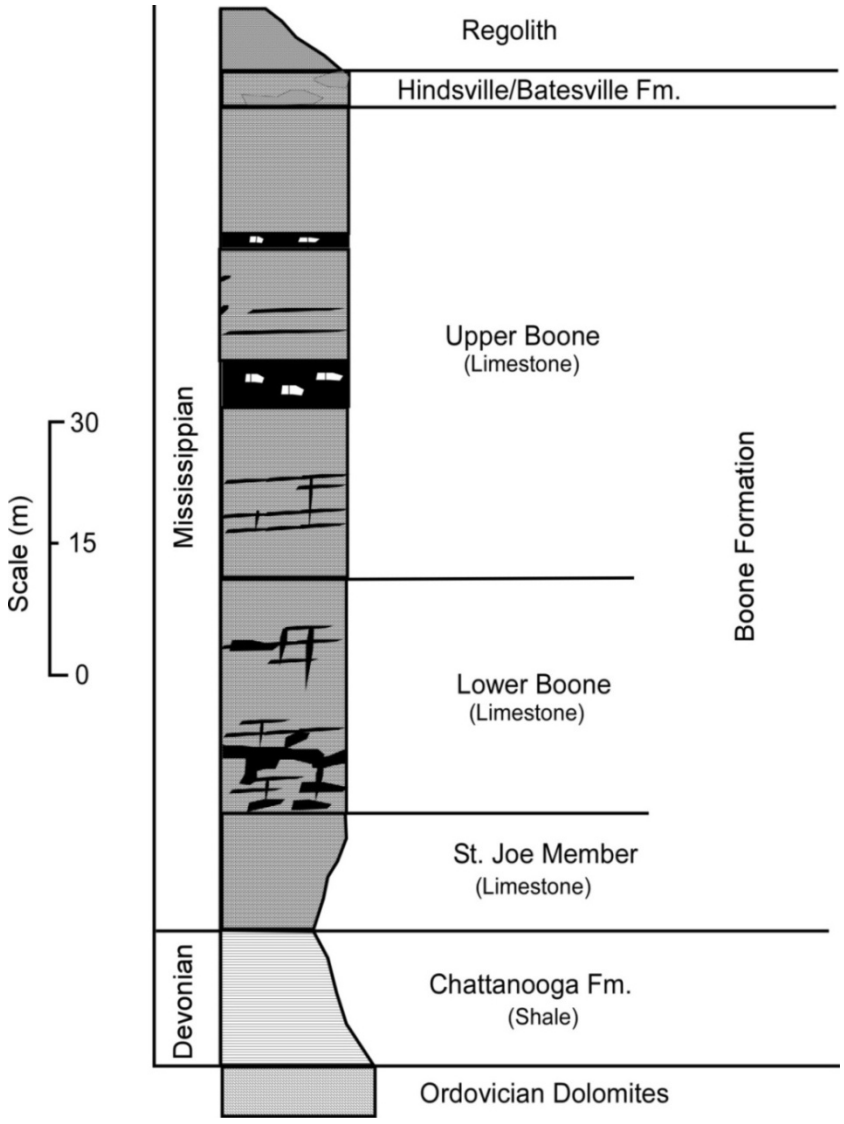

Figure 6: Stratigraphic column of NW Arkansas bedrock geology. Research site consists of Mississippian Age carbonate rock found in the Boone Formation (modified from Phelan, 2002).

1.6 Climate

NW Arkansas has a humid temperate climate with a historic mean annual temperature of 16 °C (National Weather Station 2011). The 3 °C lowest mean monthly temperature occurs in January while the 27 °C highest mean monthly temperature occurs in July (Adamski et al. 1995). Average annual precipitation in NW Arkansas is 120 cm; however, the April-June warm period accounts for 37 of the 120 cm (Adamski et al. 1995).

CHAPTER II

METHODS

2.1 Thermal Loggers

Research on thermal tracers and classification of groundwater thermal signatures in karst aquifers by Luhmann et al. (2011) serves as the primary source of information and/or background for the NW Arkansas investigation. However, not only does a distinct variation in the method of data collection exist but also geographical location. Research in NW Arkansas installed thermal data loggers in observation wells and spring outlets, while Luhmann et al. (2011) used caverns and springs in SE Minnesota. Varying collection techniques and climate differences may potentially have an impact on groundwater thermal signatures.

In the NW Arkansas investigation, monitoring equipment consisted of HOBO® Pendant Temperature/Light Loggers (UA-001-64), Stow Away TidbiT Temperature Loggers®, and Solinst Leveloggers®. Securing and fastening the equipment in observation wells and spring locations was achieved by applying extra strength trilene, galvanized wire, zip ties, catfish yarn, and duct tape. HOBO and TidbiT loggers recorded temperature while Solinst pressure transducers recorded both temperature and water level (Table 1). A Solinst logger monitored deep wells 72 and 80. In addition, a thermal logger monitored deep wells 69, 70, and 72 (Figure 7a).

Monitoring the epikarst region, seven shallow observation wells were each installed with a thermal logger. In regards to depth, deep wells ranged from depths of 50-75 (m) while shallow wells ranged from 5-10 (m). A Solinst logger was installed in both Langle and Copperhead springs while thermal loggers monitored five epikarst springs (Figure 7b): Tree, Woodpecker, Memory, Dribblin, and Red Dog. Three shallow observation wells located in alluvium (Well 4, Well 5, and Well 6) were monitored by three thermal loggers. A surface stream near the epikarst springs was monitored by a light and temperature logger.

The research period was designed to incorporate the highest rainfall months in NW Arkansas in order to monitor groundwater temperature and spring response to large precipitation events. Therefore, temperature and pressure measurements were recorded at a 15 minute interval from March 2011 - August 2011. In addition to the thermal data, other key parameters were documented. A centrally located weather station (Figure 7a) recorded daily surface temperature and precipitation measurements. Overall, the methodology of monitoring groundwater temperature, daily surface temperature, and precipitation events provides the necessary data to assign distinct thermal signatures for each subsurface flow path.

Table 1 HOBO, TidbiT, and Solinst logger specifications (Onset® 2012).

	Resolution (°C)	**Temperature Range (°C)**	**Accuracy (°C)**
HOBO Pendant Temperature/Light (UA-001-64) ®	0.14 at 25	0 - 50	±0.47 at 25
Stow Away TidbiT Temperature Loggers ®	0.30 at 20	0 - 50	±0.40 at 20
Solinst Leveloggers ®	0.01	(-) 20 - 80	± 0.05 at -10 - 40

Figure 7: (a) Location of data loggers and the weather station within the SEW research site. (b) Enlargement of the area outlined by the red rectangle in (a), the epikarst springs are labeled with their proper identifications.

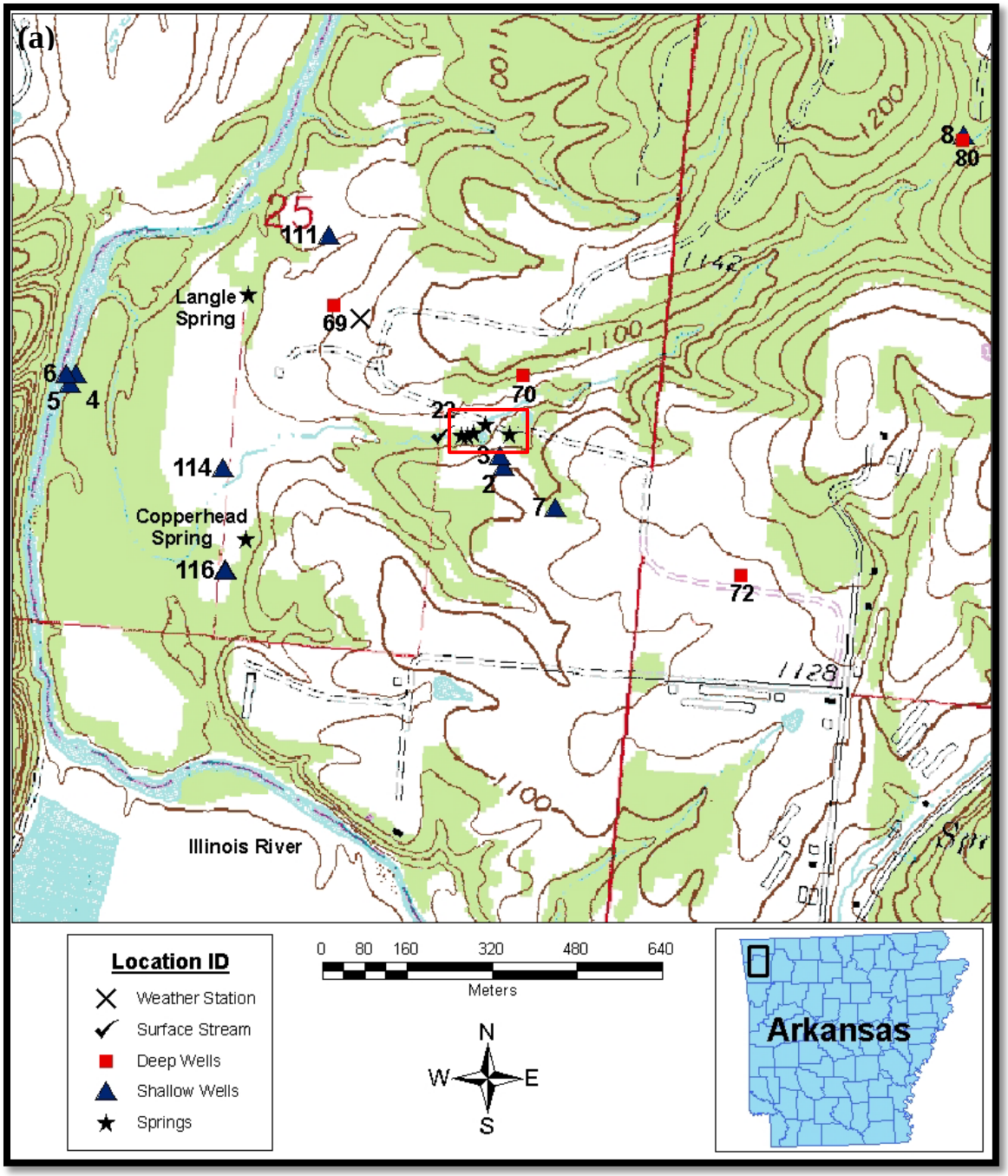
(a)
Langle Spring
Copperhead Spring
Illinois River
111
69
70
72
114
116
1
2
3
4
5
6
7
8
22
80
1100
1200
1128
Location ID
Weather Station
Surface Stream
Deep Wells
Shallow Wells
Springs
0 80 160 320 480 640
Meters
N
W
E
S
Arkansas

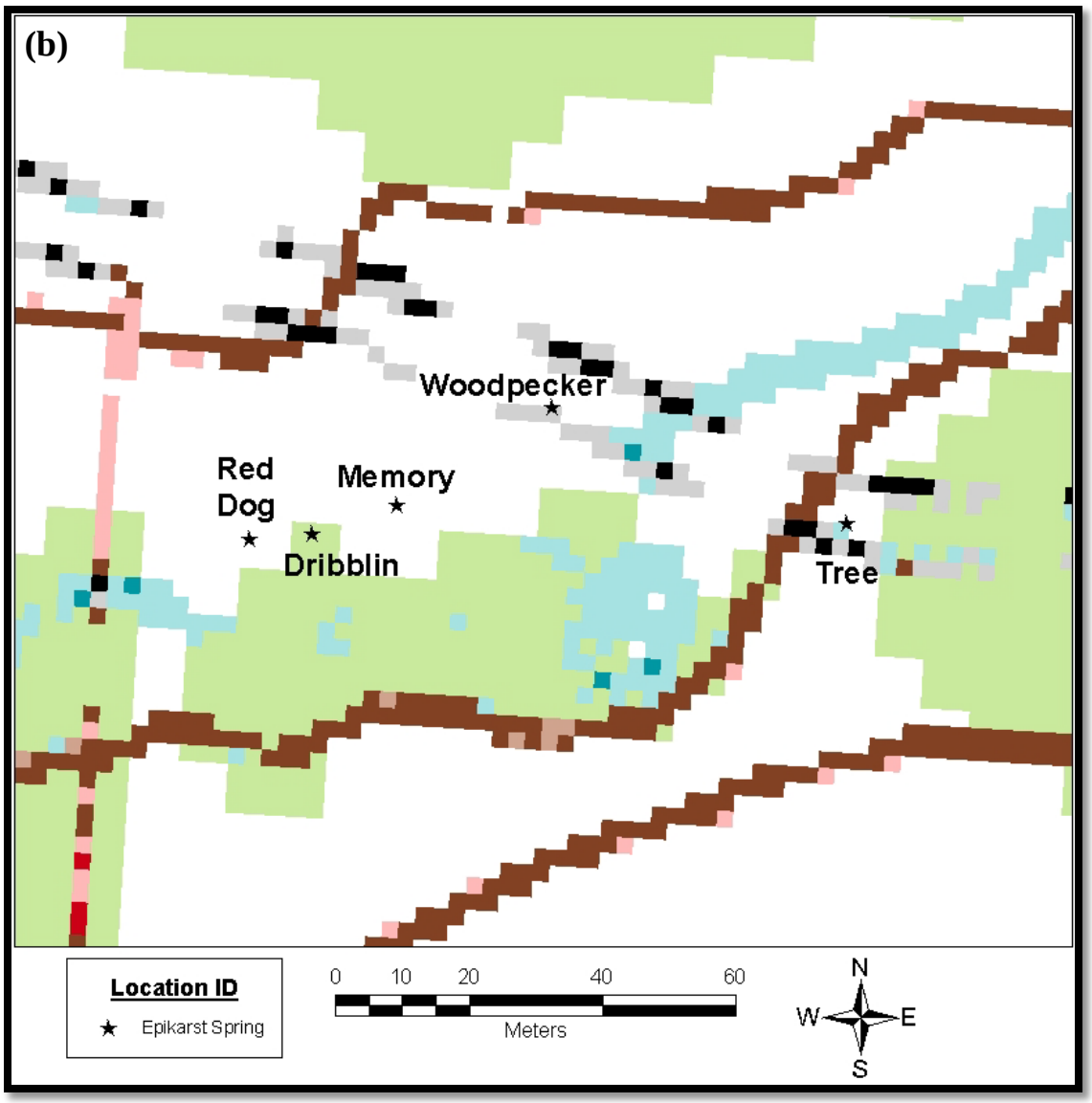
(b)
Woodpecker
Red
Dog
Memory
Dribblin
Tree
Location ID
Epikarst Spring
0
10
20
40
60
Meters
N
W
E
S

2.2 Flood Model and Visualization

In April-May 2011, NW Arkansas experienced a historic 100-year flood event. Fortunately, thermal logger equipment was installed in the subsurface prior to the significant flood event. Initial methodology planned to monitor groundwater temperatures; however, the flood event altered investigation goals. In regards to modeling the flood, preliminary concepts focused on utilizing remote sensory imagery to extract the flood's temporal progression and regression throughout the research site. The high cost and infrequent updates associated with remotely sensed imagery hindered the feasibility of this methodology. An alternative method proved necessary.

Familiarity with ESRI's ArcScene/ArcMap software produced methods that incorporated a geographic information system (GIS) as a viable option to model the historic flood event. To construct the model, several key data sources were acquired: (1) USGS Stream Gauge #07195400 data (Hubbs 2011), (2) USGS 30-m DEMs and topographic map (USGS 2010), (3) personal GPS collection of locations for each thermal data logger and/or pressure transducer, and (4) Google Earth orthoimagery (Google Earth 2011). A description of each data source and steps in the methodology are described below. Also, a flow chart (Figure 8) provides specific details for how GIS was utilized to model the spatial extent of the flood.

Stream Gauge Data: The USGS Stream Gauge #07195400 Illinois River at Hwy 16 near Siloam Springs recorded data every fifteen minutes and provided crucial insight on water level fluxes as flood waters advanced/regressed. Overall, the objective was to capture the

maximum advancement of the flood per day. Therefore, the highest daily stream gauge heights during the April 8th – May 15th period were extracted from the data file.

Topographic Map: After re-projecting the topographic map, all colors except for water bodies (i.e. blue) were removed. Following this, the topographic map was overlaid on a digital elevation model (DEM) in order to differentiate between the river channel and the floodplain. Lastly, a polygon feature class was digitized in order to outline the Illinois River channel.

Observation Well Coordinates: Prior to the flood event, a handheld Trimble GeoXH accurately (< 1m) acquired GPS points for the wells, springs, and weather station. Further, the GPS data points were imported into ArcMap. A UTM Zone 16N coordinate system, WGS 1984 datum, and a Transverse Mercator projection properly overlaid the GPS data points, DEM, and topographic map.

Flood Extent Model Derivation: Conversion of the DEM into feet allowed for the stream gauge data and the DEM to be on the similar scales. After extracting the highest daily stream gauge height, manual reclassification of the DEM (for each day of interest) was conducted. For example, all cells with values of 999 ft. (lowest elevation in DEM) to 1021 ft. (flood height as of May 15th) were reclassified as "1" or "water" while remaining cells were assigned as "0" or "non-water". Cells assigned 0 were removed, leaving only cells filled with water. Conversion of the raster layer into a polygon layer was performed in order to smooth out the flood polygon. Editing/filtering cells not connected to the main polygon was the final procedure in producing the daily flood polygon.

Visualization of Flood Extent: ArcScene was utilized to create a temporal map animation of the 2011 April-May NW Arkansas flood event. ArcScene layers, imported from ArcMap, were subdivided into three layers: Wells (GPS points), Base Layers (DEM and Illinois River feature class), and Polygons (flood polygons). In order to display the progression/regression of the flood event, individual snapshots for each polygon layer/each day of the flood event were recorded.

Moreover, the flood model output coupled with analysis of the thermal logger data throughout the flood period serves as the primary method of determining how/if the 100-year flood event impacted groundwater temperatures.

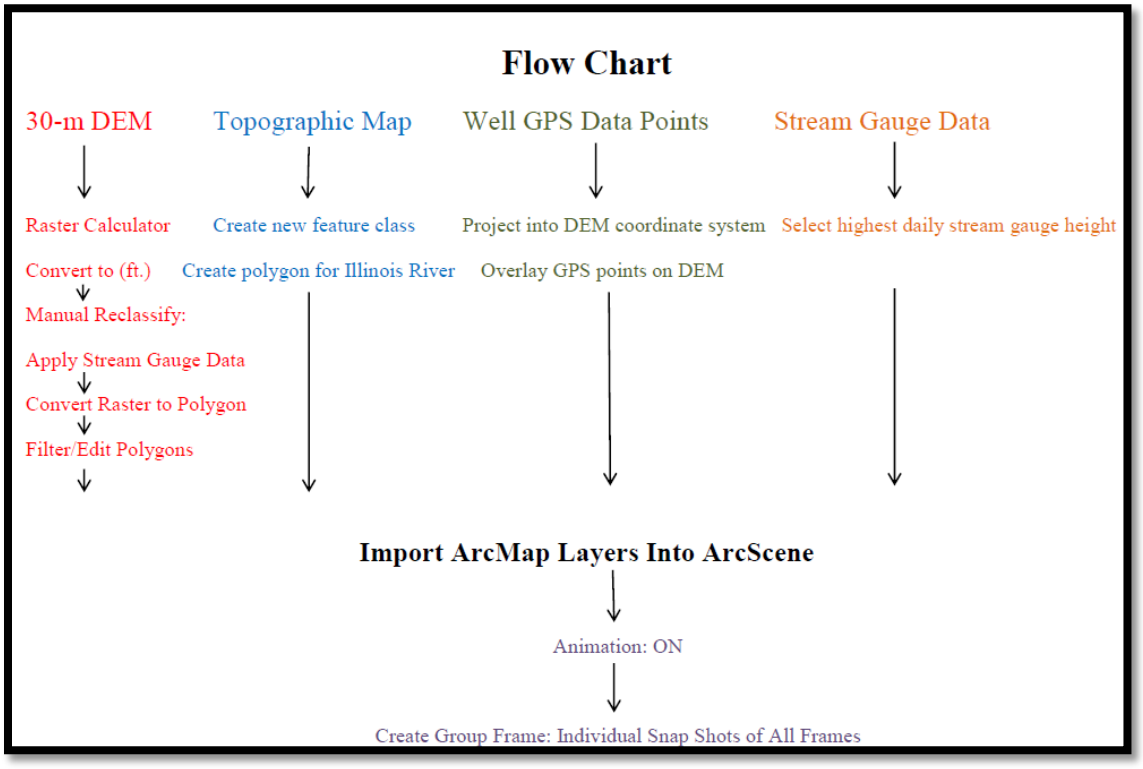

Figure 8: Flow chart depicting the major steps performed in order to produce the ArcMap/ArcScene flood model and visualization.

CHAPTER III

RESULTS: THERMAL PATTERNS AND FLOOD MODEL

3.1 Surface Air Temperature, Precipitation, and Surface Water

The 2011 March-August temperature and precipitation documentation directly corresponds to the thermal logger's installment period. Air temperature recordings were consistent with the National Weather Stations historic temperature levels while precipitation levels in Fayetteville Arkansas significantly increased (Table 2 and Figure 9). Air temperatures ranged from a minimum of 2.2 °C to a maximum of 34.4 °C. Two large scale precipitation events occurred within the investigation period: (1) April 21-27 (cumulative 29.2 cm) and (2) May 20-25 (cumulative: 19.7 cm). Note that a light and temperature logger monitored a surface stream; however, was misplaced during the recovery period (Figure 7a).

Table 2 Research period (2011 March-August) mean monthly temperature and sum of precipitation for NW Arkansas (NWS 2011).

Temperatures (˚C)

Month	March	April	May	June	July	August
Max	15.6	22.1	23.4	32.5	36.5	35.0
Mean	9.87	15.5	18.0	26.0	29.2	28.1
Min	3.89	8.54	12.3	19.3	21.8	21.3

Precipitation (cm)

Month	March	April	May	June	July	August
Sum	5.20	36.8	29.2	2.40	1.60	10.1

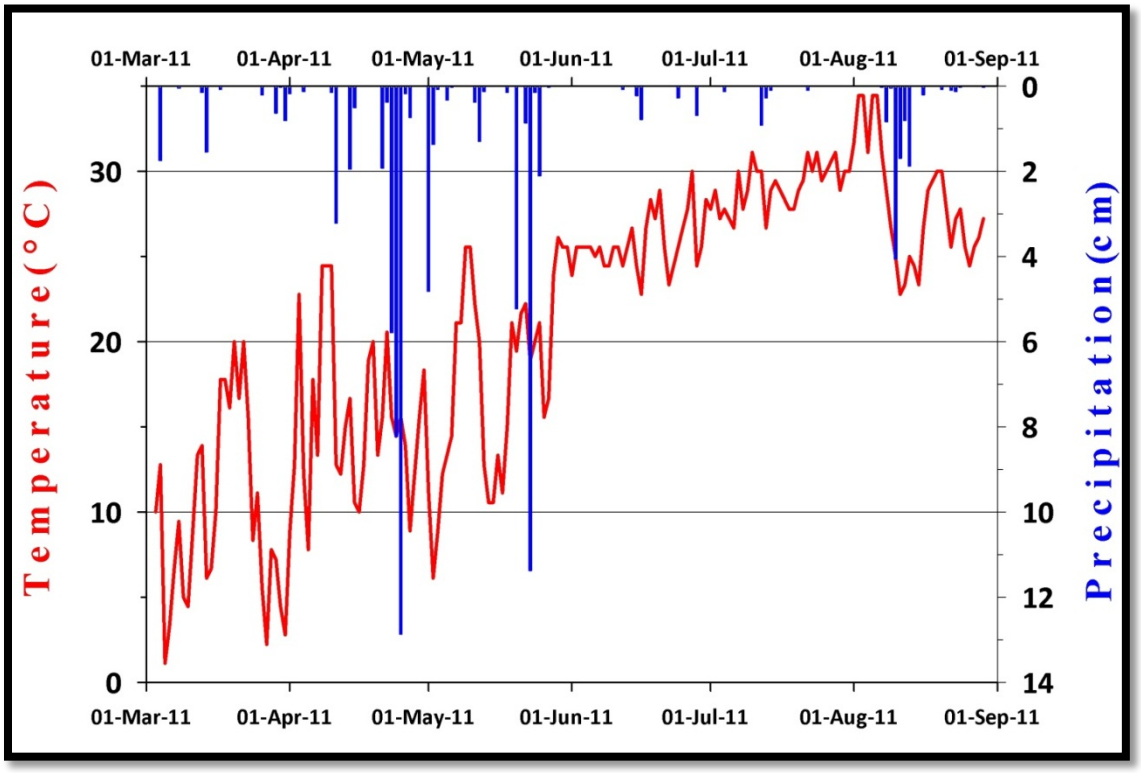

Figure 9: 2011 March 1st – September 1st surface temperature and precipitation levels for Fayetteville, Arkansas; data obtained from NWS (2011).

3.2 Thermographs and Hydrographs of Alluvium, Shallow Wells (Epikarst), Epikarst Springs, and Deep Aquifer Locations

Alluvium locations were monitored by Well 4, Well 5, and Well 6 (Figure 10a). The three alluvium locations each display a temperature signal which follows the surface air temperature trend. In addition, no diurnal signatures are noted for alluvium locations. Well 4 displays a three day 1-1.5 °C muted response to the first large-scale precipitation event in late-April while Well 6 displays a ten day 0.5 °C response. However, Well 5 thermograph displays no response to the late-April large-scale precipitation event. During the second large scale precipitation event, late-May, Well 4 responded with a 1.0 °C one day flux while Well 6 had a five day 2.0 °C temperature flux. Consistent with the previous precipitation event, Well 5 lacked a measureable response. Recovery reports on thermal data loggers installed in Well 4 and Well 6 noted that the loggers were covered in mud, not water, which may have caused the late-April temperature response whereas it is assumed that Well 5 has a better seal, ultimately reducing any thermal response to precipitation events. Alluvium's Well 6 temperature trend of 9.5–21.5 °C deviates from Well 4 and Well 5 temperature trend of 11.5-17.5 °C. A composite thermal signature was produced for the Alluvium locations, representing the average signature for Well 4, Well 5, and Well 6. The 11-19 °C positive trending temperature range closely mimics surface air temperature while also displaying a highly muted signal to precipitation events.

Comparatively, thermal loggers installed in shallow observation wells, monitoring the epikarst region at 5-10 (m) in depth, produced similar positive trending thermographs; however, certain wells display a less muted response to precipitation events. Generally, epikarst regions (Figure 10b) display both a positive temperature trend as well as a

moderate degree of fluctuation in response to precipitation events. Thermograph for Well 7 exhibits a stair-step 10-22 °C positive trending temperature signal with a maximum two-day 3.0 °C temperature response to large-scale precipitation events. Thermograph for Well 111 displays a 9.5- 21.5 °C positive trending temperature signal with a ten day 2.0 °C temperature response to large-scale precipitation events. Thermograph for Well 114 has a 12.5-18 °C positive temperature trend with minimal to no response to precipitation events. Thermograph for Well 116 has a 10.5-19.5 °C positive temperature trend with a one-five day 1.0 °C temperature flux to precipitation events. The composite of epikarst thermographs portrays an 11-20 °C positive temperature trend with a highly muted (<0.5 °C) response to precipitation events. Note that thermal loggers installed in shallow well locations Well 2, Well 3, and Well 8 either malfunctioned or were removed, providing erroneous data (Table 3).

Numerous factors contribute to the complex thermograph of epikarst spring locations (Figure 10c). All monitored locations tend to portray two significant segments: March-June and June-August. During the March-June wet period, Woodpecker, Memory, and Dribblin display a positive temperature trend with a strong diurnal temperature fluctuation. However, Red Dog's thermograph displays a relatively muted temperature signal during the same time period. During dry periods, all monitored locations mimicked surface air temperature trends while displaying relatively muted temperature fluctuations.

When recovered, thermal loggers at both Memory and Dribblin were transported from the spring orifice, but remained within the discharge flow of the spring. The duration of the displacement for Memory is unknown; however, Dribblin's displacement can be accounted for by the highly variable temperature fluctuation seen in mid-June.

Once displaced, Dribblin's thermal logger recorded surface air temperature rather than the epikarst spring's water temperature. The submerged Woodpecker location has higher amplitude in terms of diurnal temperature flux when compared to the displaced Dribblin and Memory logger recordings. The submerged logger at Red Dog spring has an anomalous thermograph signal when compared to the other nearby epikarst springs. Whereas Woodpecker, Memory, and Dribblin have approximately 11-17.5 °C temperature trends, Red Dog temperature signal ranges from 13-16.5 °C. Composite of Woodpecker, Memory, Dribblin (March-June), and Red Dog thermographs displays a 12-17 °C temperature range that mimics the positive trend of surface air temperature while also portraying a high degree of variability in response to precipitation events. Note that the thermal loggers monitoring Tree (March-April) and Dribblin (June-August) either had a general malfunction or had insufficient data due to battery loss (Table 3).

Thermographs for deep aquifer flow locations provide a relatively stable and unique signal (Figure 10d). Unconnected to surface processes, deep well locations are unaffected by fluctuations in temperature caused by air temperatures and precipitation events. The three wells, Well 70, Well 72, and Well 80, exhibit constant temperatures of 15.4 °C, 16.0 °C, and 15.4 °C, respectively. Temperature spikes of ±0.5 °C for only one reading were treated as anomalies and were ignored when generating the composite thermal signature. Deep Well 72 displays three anomalies. The first two anomalies in Deep Well 72 spike to 9.5 °C while the third anomaly records a -20 °C temperature. These three negative spikes were considered anomalies and removed from the data set. Therefore, let the near-constant 16 °C reflect Deep Well 72 temperature signal. The composite deep aquifer thermal signature maintains a stable 15.6 °C temperature. Note

that a thermal logger monitoring Well 69 was removed; assumed to be associated with a tractor accident (Table 3).

Figure 10: (a) Temperature patterns for alluvium locations; (b) temperature patterns for shallow well locations; (c) temperature patterns for epikarst spring locations; and (d) temperature patterns for deep well locations. A composite temperature pattern is included for each monitored flow path.

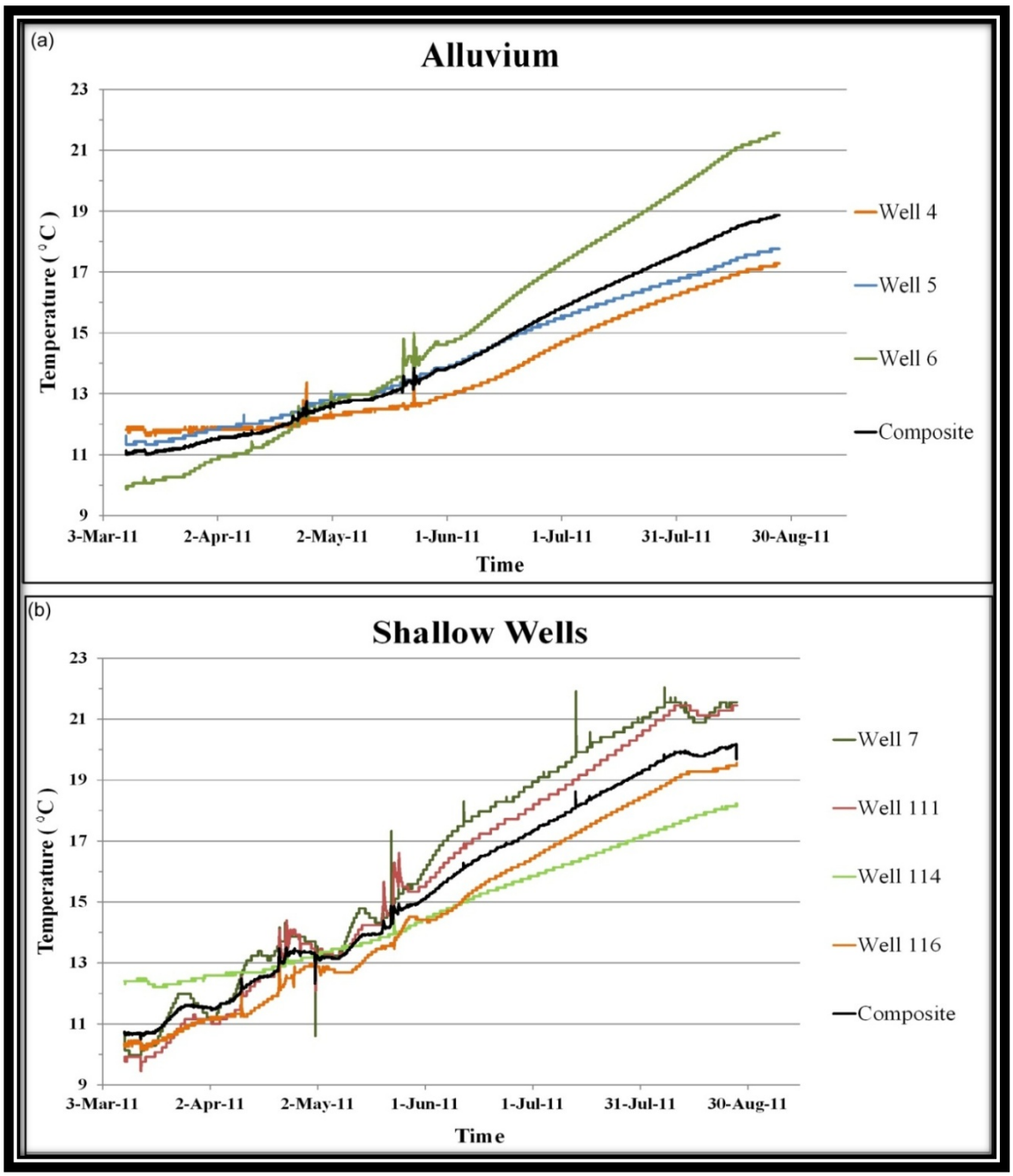
(a)
Alluvium
Temperature (°C)
23
21
19
17
15
13
11
9
3-Mar-11
2-Apr-11
2-May-11
1-Jun-11
1-Jul-11
31-Jul-11
30-Aug-11
Time
Well 4
Well 5
Well 6
Composite
(b)
Shallow Wells
Temperature (°C)
23
21
19
17
15
13
11
9
3-Mar-11
2-Apr-11
2-May-11
1-Jun-11
1-Jul-11
31-Jul-11
30-Aug-11
Time
Well 7
Well 111
Well 114
Well 116
Composite

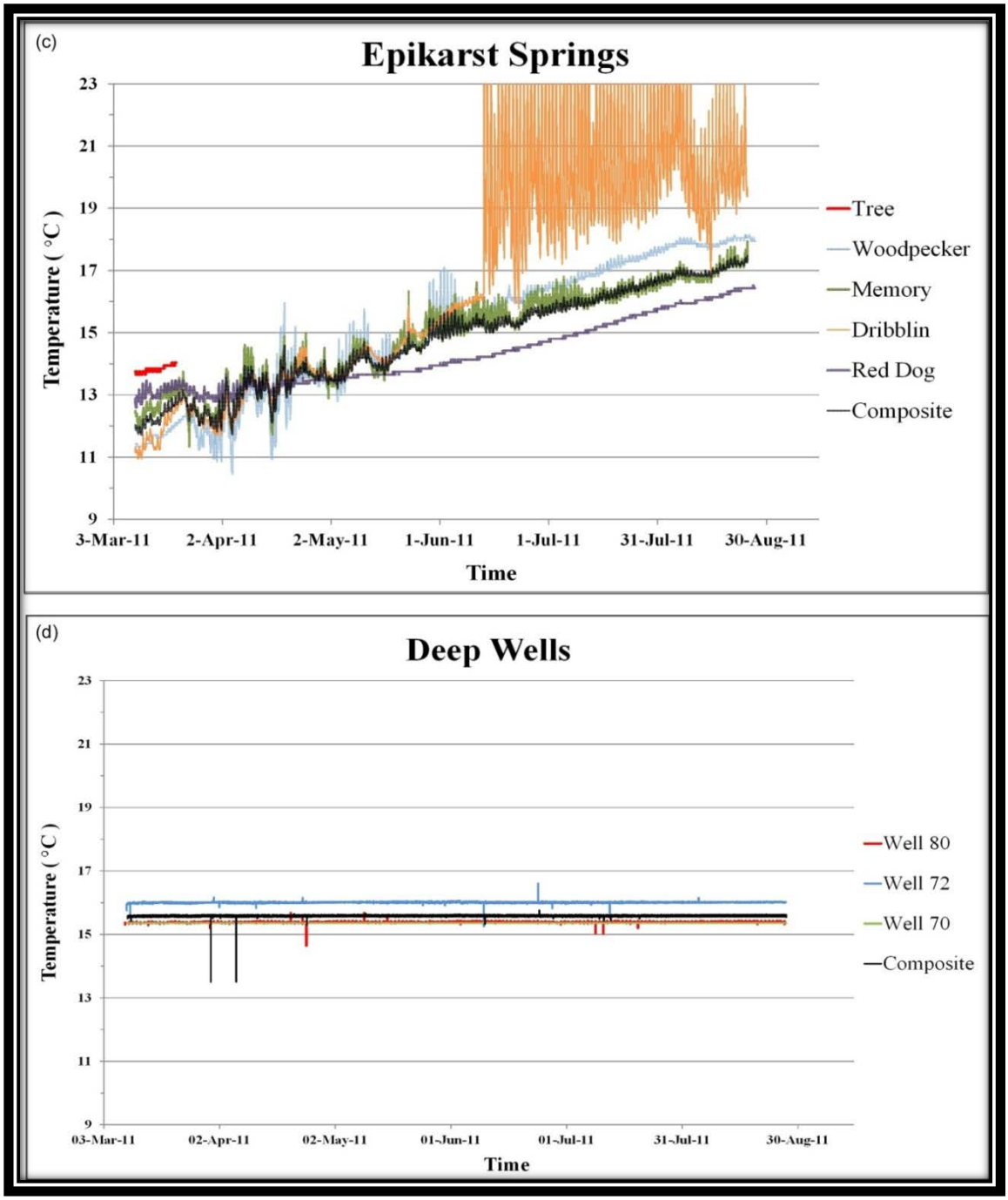
(c)
Epikarst Springs
Temperature (°C)
23
21
19
17
15
13
11
9
3-Mar-11
2-Apr-11
2-May-11
1-Jun-11
1-Jul-11
31-Jul-11
30-Aug-11
Time
Tree
Woodpecker
Memory
Dribblin
Red Dog
Composite
(d)
Deep Wells
Temperature (°C)
23
21
19
17
15
13
11
9
03-Mar-11
02-Apr-11
02-May-11
01-Jun-11
01-Jul-11
31-Jul-11
30-Aug-11
Time
Well 80
Well 72
Well 70
Composite

3.3 Langle and Copperhead Springs

The two primary discharge springs in SEW Basin 1, Langle and Copperhead, were each monitored by a thermal data logger and pressure transducer. A thermograph and hydrograph were produced for each independent spring discharge location. Thermograph Figure 11 (a) and thermograph/hydrograph Figure 11 (b-c) display the varying thermal signals for Langle and Copperhead. In the first thermograph (Figure 11a), the relatively stable Langle thermal signal is compared and/or contrasted to the saw-tooth Copperhead thermal signal. Both springs display significant responses to the large-scale precipitation events in late-April and late-May; however, the remaining portion of Langle's thermal signal is strongly muted while Copperhead's thermal signal experiences a high-degree of fluctuation. With the independent nature of both springs, it is logical that a composite signal would produce a distorted and misrepresented thermal signal. Therefore, Langle and Copperhead's data are presented individually.

Langle's thermograph and hydrograph (Figure 11b) serves the purpose of observing the interrelatedness of both the thermal signal and spring discharge level. The thermal signal at Langle spring mimics the positive trending surface air temperature. Aside from the significant responses to the two large scale precipitation events, Langle spring displays a strongly muted thermal signal. In both circumstances, late-April and late-May, Langle spring displays a sudden positive temperature spike of 1°C before returning to pre-precipitation temperatures. The late-April temperature spike is associated with a one meter increase in spring stage. No significant increase in spring stage is associated with the late-May temperature spike.

Copperhead's thermograph and hydrograph (Figure 11c) also serves the purpose of observing the interrelatedness of both the thermal signal and spring discharge level. The thermal signal at Copperhead mimics surface air temperature trends. In contrast to Langle, Copperhead displays a high degree of temperature fluctuations for the initial wet period of the investigation. Two large scale precipitation events, April 21st – 27th (cumulative 29.2 cm) and May 20th - 25th (cumulative 19.7 cm) led to both high spring stages (Figure 12) and 1 °C positive temperature spikes. The late-April temperature flux is associated with a two-and-a-half meter increase in spring stage whereas the late-May temperature flux is associated with a one-meter increase in stage.

Langle and Copperhead's individual thermal signal is further explored with a closer inspection of the spring's responses to the two main precipitation events throughout the investigation period: late-April and late-May. For the first event, Langle and Copperhead both display positive temperature spikes on April 22nd. The main difference in behavior is either the lag time or duration of the response. Langle records a maximum temperature flux of 1 °C on April 30th before returning to pre-precipitation temperatures. Comparatively, Copperhead also records a 1 °C temperature flux; however, the maximum temperature flux occurred on April 25th, five days prior to Langle (Figure 11a). A similar trend is seen during the second large-scale precipitation event. Langle and Copperhead both display initial responses on May 21st; however, Langle's temperature flux is lagged and peaks on May 28th while Copperhead's temperature peaks on May 25th. In both circumstances, one may view Langle's temperature flux as a prolonged response or a lagged response in comparison to Copperhead's thermal signal.

Table 3 Thermal data logger and pressure transducer functional report.

Site ID	Thermal Logger	Functional Report	Pressure Transducer	Functional Report
2	X	GM		
3	X	GM		
4	X	FF		
5	X	FF		
6	X	FF		
7	X	FF		
8	X	BE		
69	X	GM		
70	X	FF		
72	X	FF	X	FF
80	X	FF	X	GM
111	X	FF		
114	X	FF		
116	X	FF		
Langle	X	FF	X	FF
Copperhead	X	FF	X	FF
Tree	X	BE		
Woodpecker	X	FF		
Memory	X	FF		
Dribblin	X	BE		
Red Dog	X	FF		
Surface Stream	X	GM		
***Fully Functional (FF)**				
***Battery Error (BE)**				
***General Malfunction (GM)**	Misplaced during recovery, removed during investigation, or un-submerged.			

Figure 11: (a) Thermograph comparing/contrasting Langle and Copperhead springs. Arrows highlight the initial response of both springs to large-scale precipitation events as well as the date at which the maximum temperature flux occurred, (b) Langle Spring thermograph and hydrograph, and (c) Copperhead Spring thermograph and hydrograph. Note that the colored arrows and colored y-axis labels correspond to the graph colors for (a), (b), and (c).

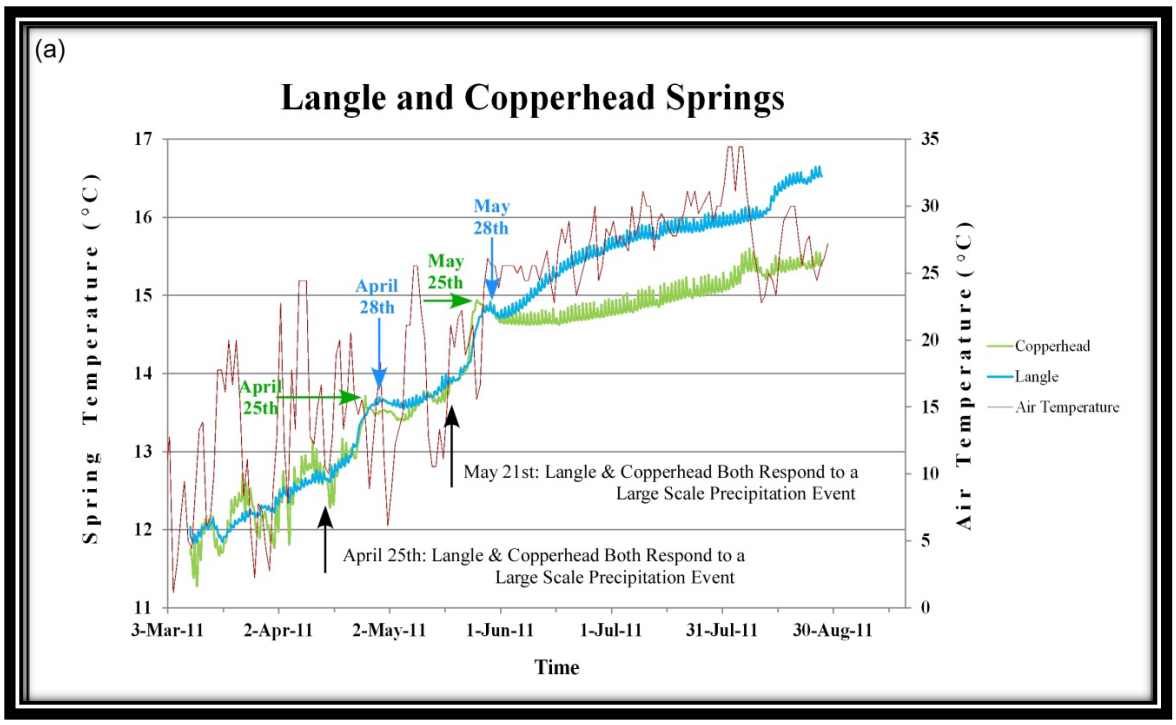
(a)
Langle and Copperhead Springs
Spring Temperature (°C)
Air Temperature (°C)
17
16
15
14
13
12
11
35
30
25
20
15
10
5
0
May 28th
May 25th
April 28th
April 25th
May 21st: Langle & Copperhead Both Respond to a Large Scale Precipitation Event
April 25th: Langle & Copperhead Both Respond to a Large Scale Precipitation Event
Copperhead
Langle
Air Temperature
3-Mar-11
2-Apr-11
2-May-11
1-Jun-11
1-Jul-11
31-Jul-11
30-Aug-11
Time

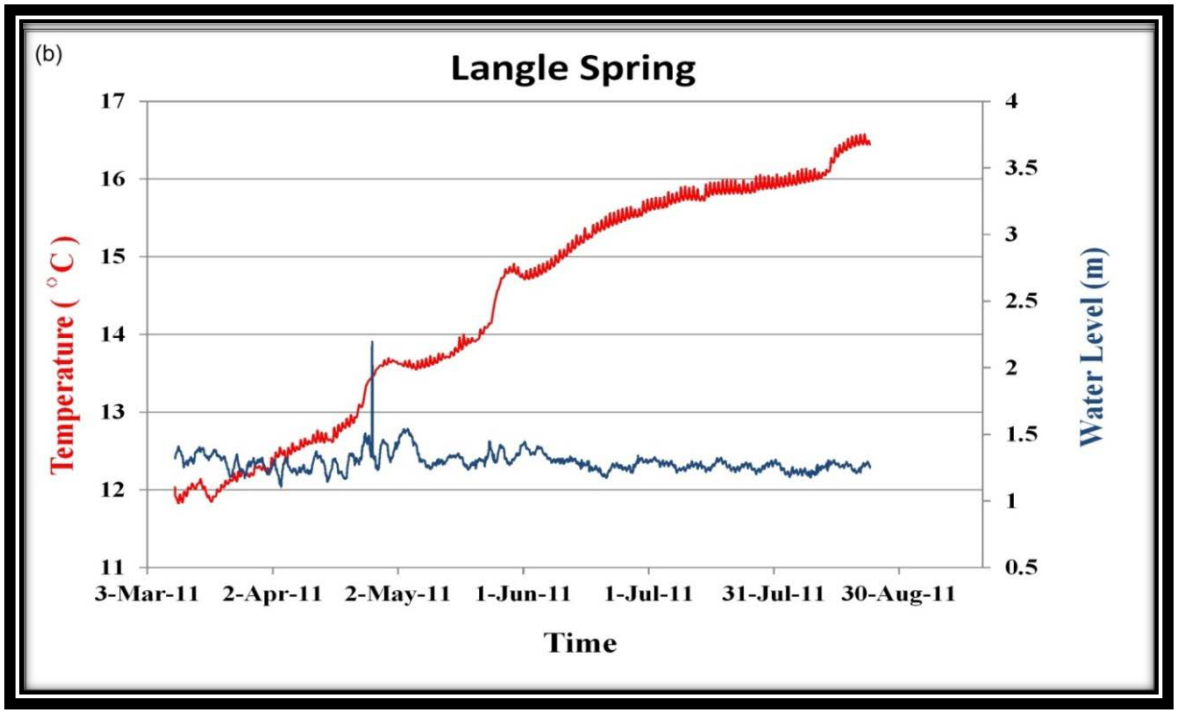
(b)
Langle Spring
Temperature (°C)
Water Level (m)
17
16
15
14
13
12
11
4
3.5
3
2.5
2
1.5
1
0.5
3-Mar-11
2-Apr-11
2-May-11
1-Jun-11
1-Jul-11
31-Jul-11
30-Aug-11
Time

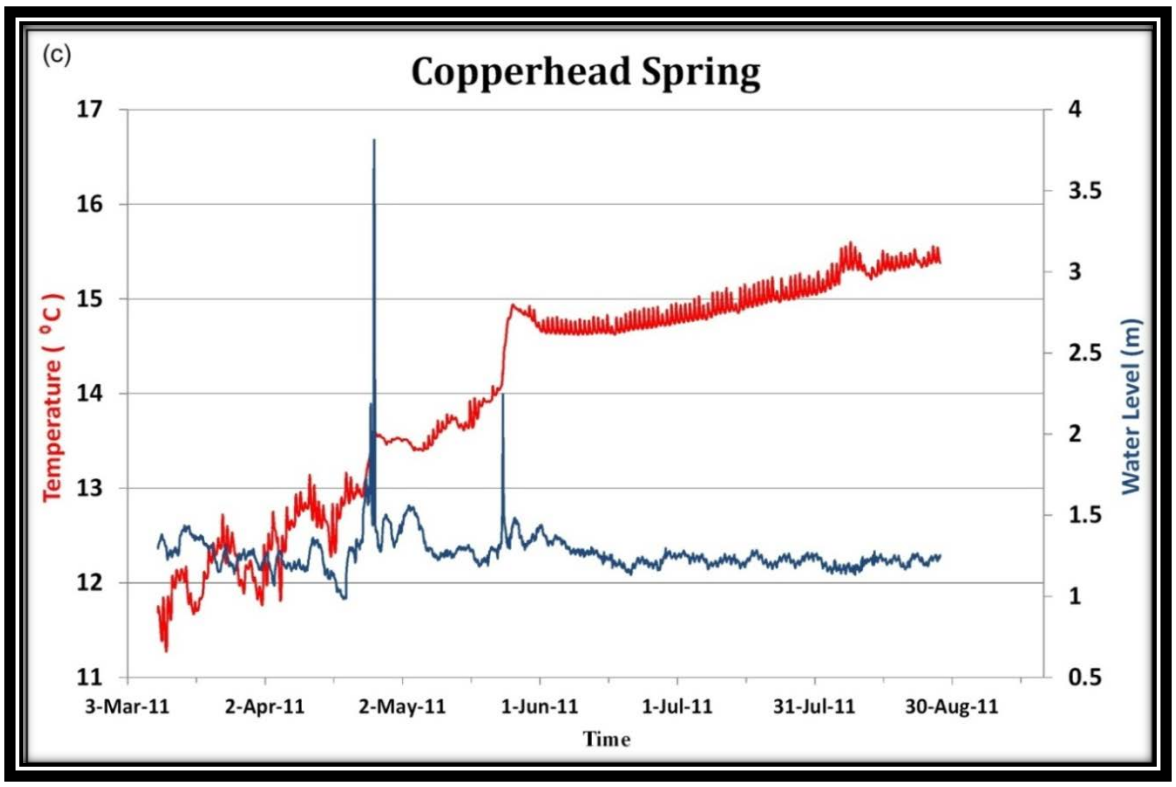
(c)
Copperhead Spring
Temperature (°C)
Water Level (m)
17
16
15
14
13
12
11
4
3.5
3
2.5
2
1.5
1
0.5
3-Mar-11
2-Apr-11
2-May-11
1-Jun-11
1-Jul-11
31-Jul-11
30-Aug-11
Time

Figure 12: Discharge from Copperhead Spring (a) March 9th 2011 low-flow conditions and (b) May 9th 2011 high-flow conditions.

3.4 Flood Model

In April-May 2011, NW Arkansas experienced a 100-year flood event. Despite the less than one percent chance of capturing the flood's thermal signature, thermal investigation equipment was installed and captured the thermal activity of the record flood event. Modeling the significant event was conducted in attempts to provide information on the flood's thermal impact on groundwater temperatures.

Construction of an ArcScene/ArcMap flood model produced a graphical portrayal of the maximum flood extent throughout the April 16th – May 6th investigation period. For orientation, Figure 13 details the general flow direction of the Illinois River and the specific location of thermal loggers in proximity to the river channel. Further, Figure 14 details the floods maximum extent per day. Flood waters breached the Illinois River channel banks and advanced onto the flood-plain throughout April 16th – April 27th. Within the SEW research site, furthest advancement of flood waters occurred on April 26th – 27th, flooding all of the following monitored locations: Langle, Copperhead, Well 4, Well 5, Well 6, Well 114, and Well 116 (Figure 14g). April 27th – May 2nd marks the period when precipitation levels decreased and floods waters retreated. However, precipitation increased during May 2nd - May 3rd and the flood waters re-advanced into the research site.

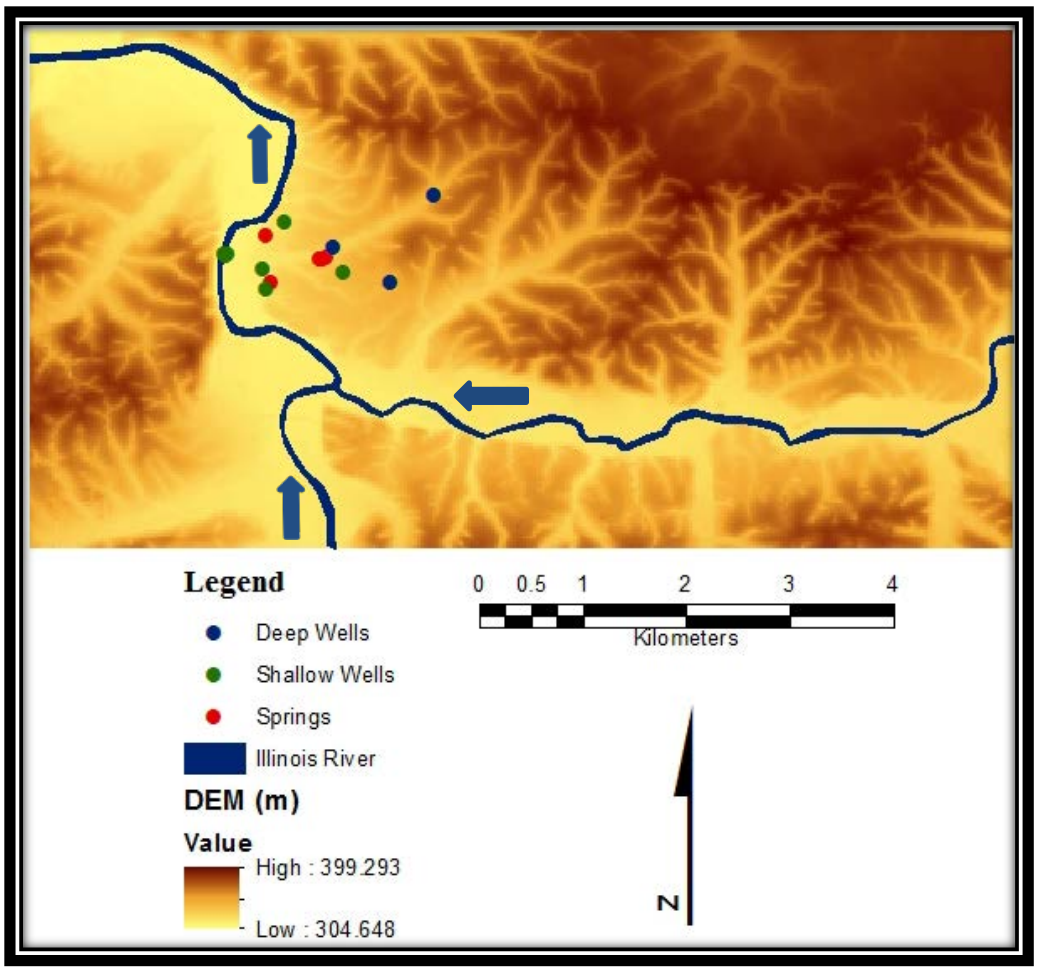

Figure 13: Compilation of the base DEM layer, well site location, and flow lines (blue arrows) of the NW Arkansas Illinois River.

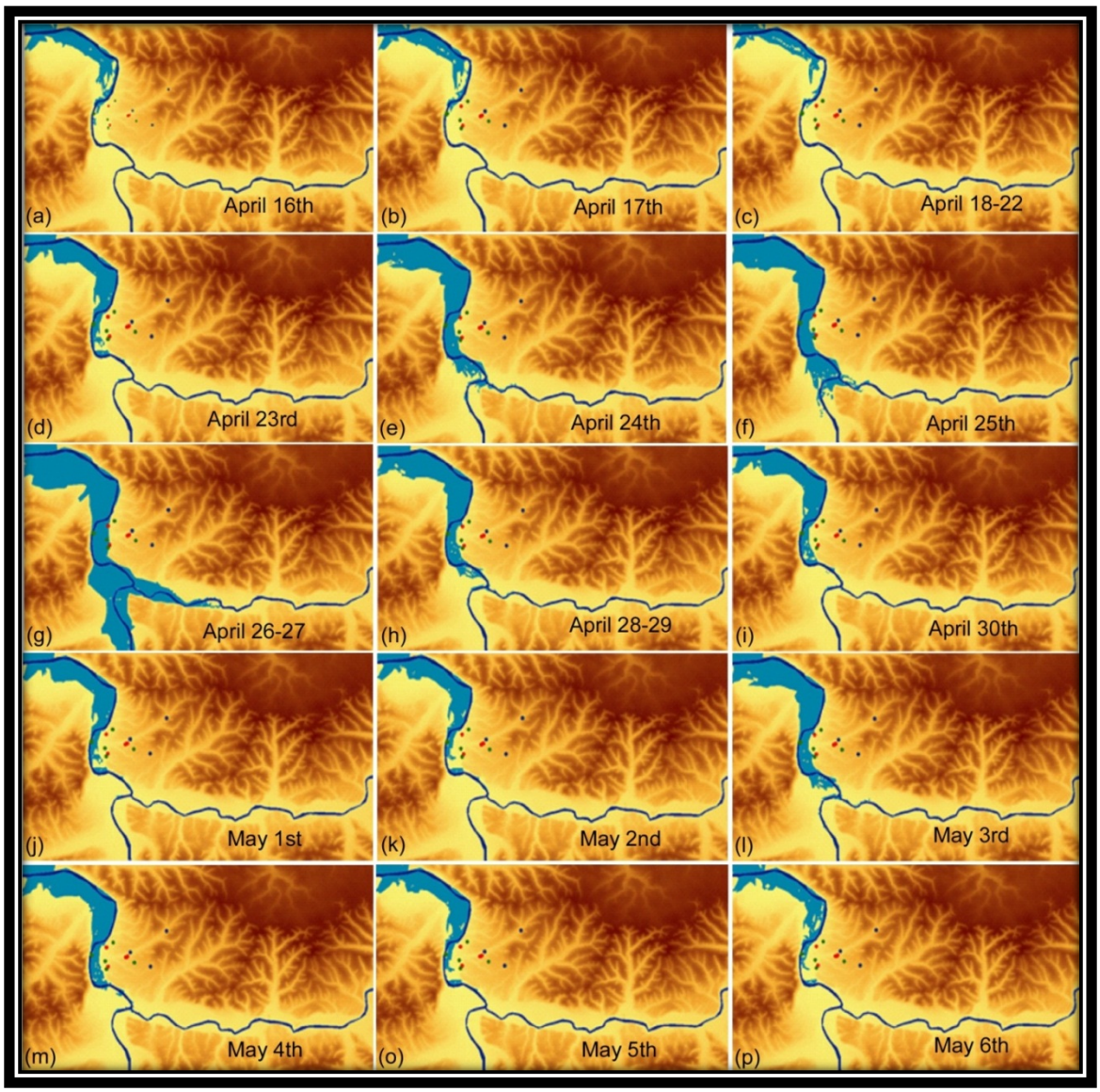

Figure 14: An ArcScene/ArcMap model and visualization of the 2011 April 16th – May 6th flood event. Each individual figure represents the highest daily advancement of the flood. Consecutive days, figures (c) and (g), are used to express days in which the flood advancement remained constant.

Of specific interest is the April 21st – April 27th time period (Table 4). The first five days within this period produced 31.29 cm of rainfall and the maximum peak of the flood pulse. The strong pulse of precipitation contributed not only to the initial breach of water from the river channel, but also the temperature spike in groundwater (Figure 15).

Monitored locations, Langle, Copperhead, Well 4, Well 6, and Well 116 all display positive temperature spikes during the April 22nd – April 26th time frame period highlighted in Figure 15. The final two days contributed a combined 1.15 cm of rainfall (Table 4) and the substantial decrease in rainfall should have ceased groundwater temperature fluctuations; however, thermographs continue to show fluctuating signals (Figure 15). The flood model in Figure 14 (g) confirms that flood waters remained over certain Alluvium, Shallow Well, and Spring locations causing the temperature fluctuation to persist. As precipitation decreased, flood waters retreated and the temperature signals return to pre-precipitation/flood conditions.

Table 4 Recorded precipitation levels for April 21st – 27th 2011 (NWS 2012).

Date	Precipitation (cm)
21-Apr	1.93
22-Apr	0.51
23-Apr	7.77
24-Apr	8.66
25-Apr	12.42
26-Apr	0.08
27-Apr	1.07

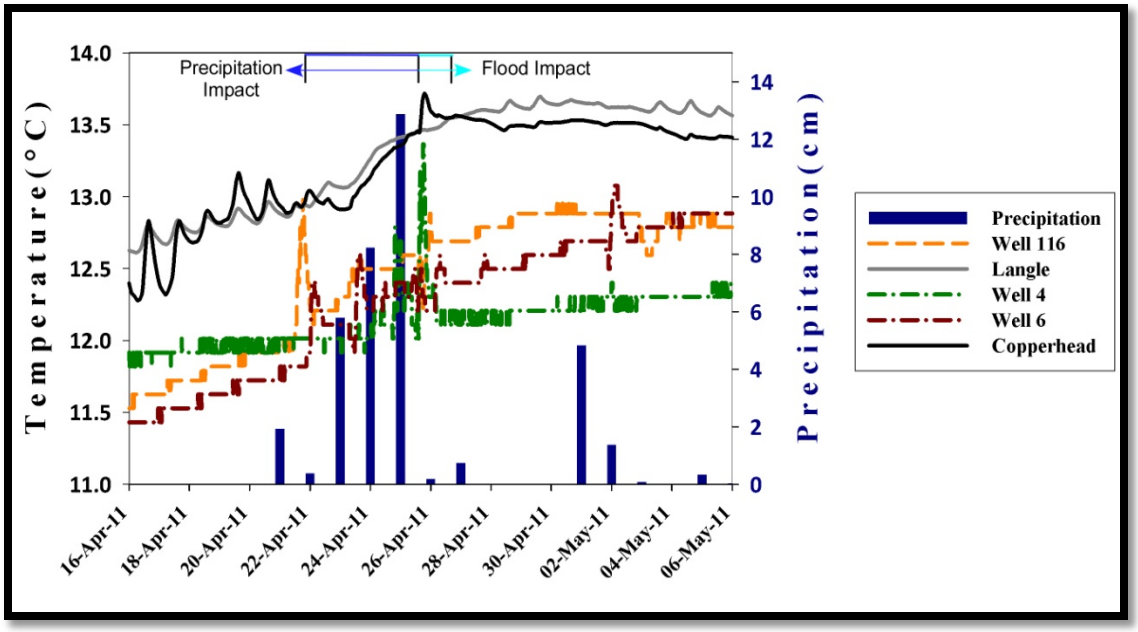

Figure 15: Thermal impact of a combined large-scale precipitation and 100-year flood event. Note that the top color coded arrows correspond to the x-axis time period and the mechanism that produced the groundwater response; solid lines represent Spring locations; the dashed line represents a shallow well (epikarst) location; and the dashed-dotted lines represent Alluvium wells.

CHAPTER IV

DISCUSSION: THERMAL PATTERNS AND FLOOD MODEL

4.1 Surface Air Temperature and Precipitation

For the 2011 March-August research investigation period, surface air temperature displayed a strong positive trend. Temperature steadily increased through July (Table 2), reaching a mean 29.2 °C temperature for the month. In relation to the historic mean 27 °C temperature for July, the 2011 investigation period's surface air temperature is within the expected range. On the other hand, precipitation measurements strongly deviated from historic averages. As previously mentioned, average annual precipitation measurements hover around 120 cm. During the 2011 investigation, April and May alone accounted for 60 cm of rainfall. Rainfall is a unique parameter to consider when conducting a thermal investigation because of its ability to retain/store the surface air temperature. Dependent on location and time of year, recharging warm or cold rainwater will impact subsurface water temperatures. For example, during warm periods rainfall retains a warm temperature, producing a positive thermal spike for groundwater when mixed. Likewise, during cold surface conditions, rainfall retains the colder temperature and creates a negative thermal spike when recharging surface waters mix with groundwater. Therefore, these anomalous precipitation measurements are invaluable when designating thermal signatures for various flow components.

4.2 Thermal Classification of Alluvium, Shallow Wells (Epikarst), Epikarst Springs, and Deep Aquifer Locations

Properly functioning thermal equipment recorded various groundwater flow temperatures throughout the entire aquifer system. Plotting thermal signals on thermographs and hydrographs reveal distinct thermal signatures. Specifically, the thermograph/hydrograph combination produce three distinct thermal patterns (Figure 16) for various flow paths along the SEW karst aquifer. Pattern 1 (ineffective heat exchange) portrays high temperature variability in response to precipitation events while in-phase with surface air temperature. Pattern 2, from here forth referenced as *mixed*, is a combination of effective and ineffective heat exchange groundwater flow. The mixed signal displays muted temperature fluctuations to precipitation events while being in-phase with surface air temperature. Pattern 3 (effective heat exchange) is a long-term stable temperature unaffected by seasonal fluctuations in surface air temperature or precipitation events. In relation to Luhmann et al. (2011) thermal investigation, two of the three previously mentioned thermal signatures are comparable (ineffective and effective). However, Luhmann et al. (2011) created two subdivisions for ineffective and effective heat exchange while present thermal investigations revealed a *mixed* flow component.

Epikarst spring's thermal signature is produced in environments where recharging waters traverse through the aquifer system at rates which inhibit thermal equilibrium. Groundwater discharging at epikarst spring locations retains the surface air temperature signal while also containing a strong response to precipitation events. Water retaining the surface air temperature signal indicates a short flow path from surface input locations to groundwater output locations. The high variability seen in the epikarst spring

thermograph, exemplified by the saw-tooth pattern, is produced by the diurnal effect (e.g. recharge waters retain both the daily warm period temperatures and colder nightly temperatures). For the SEW investigation, Epikarst springs display the strongest ineffective heat exchange thermal signature (Pattern 1). In relation to Luhmann et al. (2011) research, epikarst springs would be equivalent to the Event-Scale Variability (Pattern 1) signature.

Groundwater temperatures that mimic surface air temperatures occur when there is a short connection/flow path between the infiltrating waters and the subsurface. The short connection, and therefore short groundwater residence time, allows the infiltrating waters to retain the surface air temperature. Both epikarst and alluvium regions, monitored by shallow wells, contain groundwater temperature signals that resemble the positive trending surface air temperature. However, both regions are designated as a mixed thermal pattern due to the combination of the positive trending temperature and muted response to precipitation events. The muted response to precipitation events indicates a degree of prolonged groundwater residence time. Extending recharge residence time produces an environment where groundwater has the ability to equilibrate with the surrounding geologic material. Overall, shallow well (epikarst) and alluvium locations are defined as a mixed (Pattern 2) thermal signature due to their dual components of (1) short connection between surface waters and groundwater and (2) muted response to precipitation events.

Flow systems where groundwater and the surrounding bedrock effectively transfer heat and reach thermal equilibrium are designated as Pattern 3. The depth at which the deep well locations monitored groundwater flow is a crucial parameter to

consider when assigning deep aquifer locations thermal signature. Slow groundwater movement, found in deep aquifer locations, are at such depths where surface processes (e.g. surface temperature or precipitation) have limited to no impact on groundwater temperature. In other words, deep aquifer locations possess an *unconnected* component. The unconnected component coupled with long groundwater residence time (e.g. surface waters percolating/infiltrating through the soil/regolith horizon, stored/vertically transferred through epikarst regions to eventual deep aquifer flow locations) produce a near constant groundwater thermal signal. Therefore, deep aquifer locations are assigned a strong effective heat exchange thermal signature (Figure 16). In relation to Luhmann et al. (2011) research, deep aquifer flow within SEW Basin 1 would be equivalent to the Constant Aquifer Temperature (Pattern 4) signature.

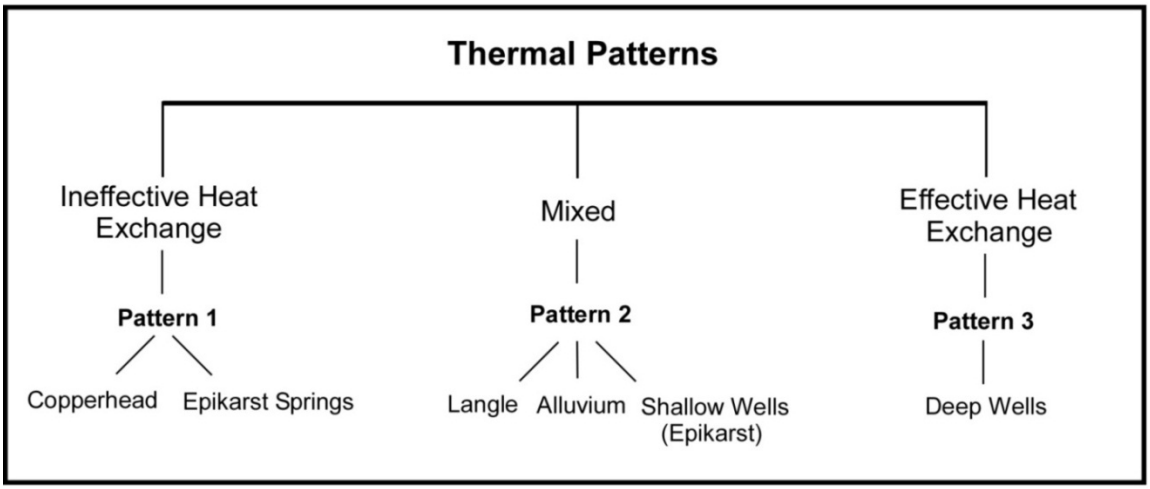

Figure 16: Flow chart delineating the three groundwater thermal signatures.

4.3 Langle and Copperhead Springs

Since the two primary discharge locations in Basin 1 are separated by a mere 300-400 (m) one may falsely assume that the thermal signatures for Langle and Copperhead should act similarly. However, this is not the case. Two conceptual models (reference Brahana et al., 2005 Figures 9 & 10) detailing the hydrogeological connection between Langle and Copperhead springs may potentially provide insight on the processes which cause Langle and Copperhead to differ thermally.

During the March-June 2011 investigation period, Langle's water temperature is relatively muted when compared to Copperhead's saw-tooth fluctuations. The phenomena can be explained by the conceptual model while also factoring in the warm wet period under observation. Copperhead spring receives the bulk of recharging waters after precipitation events. Therefore, it is logical to deduce that Copperhead's saw-tooth thermal signal is associated with the following mechanism: short groundwater residence time. Copperhead's saw-tooth thermal pattern may partially originate from the epikarst spring discharging waters which flow down gradient into one of the few existing surface streams within the research site. The thermally ineffective epikarst spring water flows to a nearby influent stream, potentially contributing a fraction of water to the nearby Copperhead spring. Overall, short groundwater residence associated with the precipitation → epikarst → epikarst springs → influent surface stream → Copperhead spring flow path may contribute to Copperhead's saw-tooth thermal signal.

Langle's thermograph displays low variability during the same time period. Further analysis of the conceptual model may also account for this occurrence. Ting (2005) describes how recharging waters are delayed and/or ponded due to a subsurface

storage component (e.g. calcite growth, debris dam, or mud dam). During the wet season, ponded groundwater rises to a level where an overflow conduit directs the water to Copperhead (Figure 17). This accounts for Copperhead saw-tooth thermal signal during high flow periods (retaining the diurnal surface air temperature), while base flow conditions (relatively stable and lagged thermal signal) contribute water to Langle.

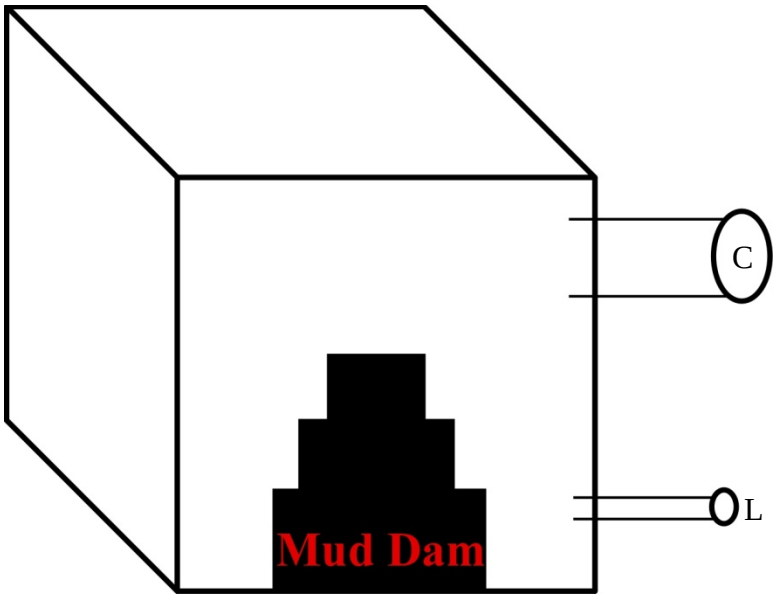

Figure 17: Conceptual model of a conduit passage which contains a storage component (e.g. a mud dam). During high flow conditions, majority of groundwater discharges at Copperhead. Under low flow conditions, groundwater primarily discharges at Langle.

Under low flow conditions, Langle serves as the primary discharge location for Basin 1. According to Ting (2005), Langle discharges 3.96 X 10^{-4} m^3/s during base flow conditions, twice as much discharge as Copperhead's 1.98 X 10^{-4} m^3/s. Base flow conditions account for the thermal signal observed in Langle's hydrograph and thermograph. In comparison to Copperhead, Langle's thermograph is slightly lagged in response to precipitation events (Figure 11a). Ting's (2005) conceptual model

hypothesizes that Copperhead receives water from an overflow conduit, which confirms that Copperhead's thermograph should respond first to precipitation events. As precipitation ceases, water level drops below the overflow conduit tube and flow is directed towards Langle.

Overall, three components (1) lag time relative to Copperhead (2) muted response to precipitation events and (3) temperatures which mimic surface air temperature trends are all used to designate Langle's system as a mixed thermal signature. On the other hand, Copperhead's components of a direct response to precipitation events, the diurnal or highly variable temperature fluctuations, and a temperature trend which mimics surface air temperature produce a strong ineffective heat exchange thermal signature.

4.4 Composite Discussion

Each groundwater flow path (e.g. alluvium, shallow wells (epikarst), epikarst springs, deep aquifer, and springs) was monitored by multiple thermal loggers. Although multiple loggers monitored each individual flow path, the installment depth, geographical location, and degree of saturation were several factors which may have produced varying thermal results. Methodology of creating a composite thermal signal appeased the process of assigning a unique thermal signature for each individual flow path (Figure 18).

For example, creation of a composite signature served the purpose of grouping the deep aquifer flow locations (Well 70, Well 72, and Well 80) to a single thermal signal. Well 70 and Well 80 had a near constant 15.4 °C temperature range while Well 72 maintained a near constant 16 °C temperature. Averaging the three locations together

produced one composite deep aquifer thermal signature of 15.6 °C. The composite deep well location strongly represents an effective heat exchange thermal pattern.

Similar methods were applied to shallow wells (epikarst), alluvium, and epikarst spring flow. In these locations, the composite signature maintained the thermal signal as seen in the individual thermographs. Composite thermal signatures for shallow wells (epikarst) and alluvium locations are indicative of a mixed thermal pattern. Both locations have a muted temperature response to precipitation events while also mimicking the positive trend of surface air temperature. As for epikarst spring flow, the composited thermal signal is dampened from July-August but the initial March-June signal strongly displays ineffective heat exchange. Note that the epikarst spring composite retains the high degree of temperature fluctuation in response to rainfall events, whereas other composite signals tend to lose their ineffective heat exchange characteristic once composited.

Langle and Copperhead springs were not composited. The thermal composite signal for Langle and Copperhead produced a misleading non-representative thermal signature. The SEW Basin 1 conceptual model (reference Brahana et al., 2005 Figures 9 & 10) supports the decision of designating Langle and Copperhead as different flow components. Langle represents a mixed thermal signature while Copperhead strongly represents an ineffective heat exchange thermal signature. If composited, Langle springs mixed nature dampens and reduces the true ineffective heat exchange nature of Copperhead spring. However, the two primary discharge springs in Basin 1 are significant, therefore are included on the composited thermograph for comparison purposes.

Overall, each monitored location represents either ineffective heat exchange (Pattern 1), mixed (Pattern 2), or effective heat exchange (Pattern 3) (Figure 16). However, alternative composite thermal signatures may be produced if research is conducted in varying geographic locations, temperature climates, or maturity levels (epikarst regions).

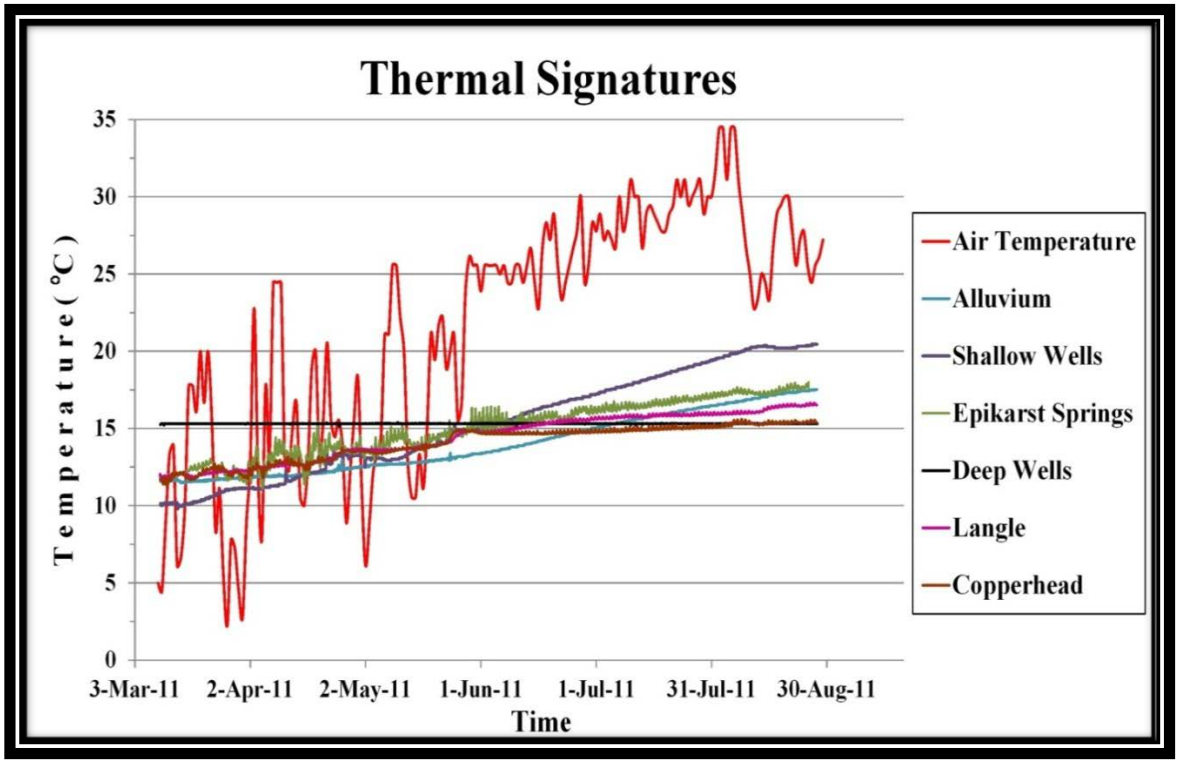

Figure 18: Thermograph of the composite signatures for each individual flow component.

4.5 Flood Model

ArcScene and ArcMap modeling of the 2011 April-May flood event in NW Arkansas provided potentially useful information of how surface conditions (e.g. rainfall or floods) impact the subsurface. The modeling objective was to create an accurate

visualization of the advancing and retreating floodwaters through the SEW investigation site. Analysis of the flood model and visualization coupled with the analysis of groundwater thermographs lends insight on whether the historic flood event impacted groundwater temperatures.

Prior to the discussion on whether or not the flood impacted subsurface temperatures, a brief discussion of the flood model accuracy is needed. Primary concerns within the construction of the model centered on the accuracy of the stream gauge data provided by the United States Geological Survey. Stream gauges located in near proximity of the SEW research site were washed away by the NW Arkansas 2011 historic flood event. Therefore, the closest functioning stream gauge was the USGS Stream Gauge #07195400 located in the Illinois River at Hwy 16 near Siloam Springs, 11 kilometers (km) downstream. Application of the stream gauge data 11 km downstream of the research site inherently produces a degree of error in the model. However, personal flood observations of the NW Arkansas 2011 flood event provides confirmation that the flood model is in close approximation of the floods maximum advancement.

Once the model was determined to be reliable, comparison of the floods advancement within the research site to subsurface temperature fluctuations commenced. Inspection of the maximum flood advancement on April 26^{th} – 27^{th} in relation to the well site location revealed that the surface flood waters resided over the following locations: alluvium wells (i.e. Well 4, Well 5, and Well 6), shallow wells (epikarst) 114 and 116 and both Langle and Copperhead springs. However, thermographs of these monitored locations display the initial response/fluctuation of groundwater temperature several days *prior* to the flood advancement. Therefore, an alternative process must account for the

initial groundwater spikes. The large-scale precipitation event on April 23rd – April 25th (Table 4) is determined to be the source of the initial groundwater temperature fluctuations. In seventy-two hours, 28.85 cm of rainfall was recorded. The initial temperature fluctuations are therefore related to the recharge event rather than the surface flood.

Recharging waters, retaining the surface air temperature, accounted for the initial groundwater spikes; however, precipitation relatively ceased (< 1.5 cm) for the duration of April. Interestingly, thermographs of Well 4, Well 6, Well 116, and Langle and Copperhead springs continue to show variability through April 26th – 27th. By this period, three-to-four meter high flood waters advanced several hundred meters into the research site. Since precipitation ceased and groundwater temperature signals continued to show a response, it is determined that the warm surface flood waters impaired subsurface temperatures.

Copperhead's thermograph (Figure 15) strongly displays how both the recharge event and historic floods impacted subsurface temperatures. Initial response to the rainfall event occurs April 23rd and increases through April 25th. On April 26th, the thermal signal has anomalous, rapid positive spike. The anomaly is unassociated with the recharging waters for two primary reasons: (a) precipitation levels relatively ceased on April 25th and (b) recharging waters create a consistent positive temperature trend; however, on April 26th there is a significant temperature flux which deviates from the previous set trend. This rationale linked with modeled results, that position flood waters over Copperhead on April 26th, allows for the assumption that the rapid temperature flux is associated with surface flood waters impacting Copperhead's thermal signal.

Another monitored location which strongly displays groundwater temperatures susceptibility to surface process is Well 4. Interestingly, Well 4 lacks a response to the large scale precipitation event; however, displays a direct response once the flood waters advanced over the monitored location (Figure 15). Therefore, Well 4 and Copperhead are two strong examples which confirm that certain subsurface temperatures are interrelated with surface processes. Note that Well 5 and Well 114 were anomalous among the flooded wells and displayed no significant response to either the precipitation or historic flood events. Therefore, the thermograph for Well 5 and Well 114 in Figure 15 were omitted.

CHAPTER V

CONCLUSION

When unraveling the complex subsurface flow components of a karst aquifer, the application of thermal tracers and thermographs/hydrographs has been an underutilized tool. The cost-effectiveness and non-labor intensive components are several of the attractive characteristics of a thermal investigation. Analysis and interpretation of the 2011 March-August karst aquifer investigation has classified three distinct thermal signatures: ineffective heat exchange (Pattern 1), mixed (Pattern 2), and effective heat exchange (Pattern 3). Assigning thermal signatures was primarily a function of storage and transport rates, aquifer depth, groundwater residence time, and response to precipitation events.

An ineffective heat exchange signal contains a thermal signal that mimics surface air temperature trends and has high temperature variability/fluctuations in response to precipitation events. In addition, strong ineffective heat exchange is indicative of low storage and high transport rates, shallow aquifer flow, and short groundwater residence time. In SEW Basin 1, strong ineffective heat exchange is assigned to both Copperhead and Epikarst Spring flow. Effective heat exchange occurs in aquifer flow at great depths where an unconnected nature to surface processes and long groundwater residence promote thermal equilibrium. The 16 °C near-constant deep aquifer thermal signal is representative of a strong effective heat exchange thermal signature. Combining

characteristics of ineffective and effective heat exchange produces a mixed thermal signal. A mixed signal is assigned to flow paths that mimic surface air temperature trends; however, have muted and/or lagged responses to precipitation events. A mixed thermal signature is assigned to Langle, Alluvium, and Shallow Well (Epikarst) flow paths.

Coupling subsurface thermal investigations with a surface flood model was utilized to determine the connection between surface processes and groundwater temperatures. Analysis and interpretation of the NW Arkansas 2011 100-year flood event model and groundwater thermal signals suggest that large-scale precipitation and flood events produce groundwater temperature fluctuations. Moreover, meshing the multiple components of the investigation (e.g. thermal tracing of flow at input and output locations, tracing flow as it traverses between these two locations, and incorporating a flood model to determine surface/subsurface connectedness) has verified that thermal tracers are a reliable method of assigning distinct thermal signatures to various karst aquifer flow components.

A recommendation to improve this investigation is to prolong the investigation period. Increasing the duration of a thermal investigation may potentially alter thermal pattern classification as seasonal variation and/or various recharge mechanisms are introduced.

REFERENCES

Adamski, J.C Petersen, J.C., Freiwald, D.A., and Davis, J.V., 1995, Environmental and hydrologic setting of the Ozark Plateaus study unit, Arkansas, Kansas, Missouri, and Oklahoma: U.S. Geological Survey Water-Resources Investigations 94-4022, p. 1-79.

Al-Rashidy, S., 1999, Hydrogeologic controls of groundwater in the shallow mantled karst aquifer, Copperhead Spring, Savoy Experimental Watershed, northwest Arkansas [M.S. thesis], Arkansas, University of Arkansas p. 50-74.

Al-Qinna, M., 2003, Measuring and Modeling Soil Water and Solute Transport with Emphasis on Physical Mechanisms in Karst Topography, [Ph. D Thesis] 296 p.

Bonacci, O., 1993, Karst Springs Hydrographs as Indicators of Karst Aquifers: Hydrological Sciences, v. 38, p. 51-62.

Brahana, J.V. 1997, Savoy Experimental Watershed and Field Research Facility – A Long-Term Karst Research Site: http://www.uark.edu/depts/savoyres/index.html (accessed March 2011).

Brahana, J.V. Sauer, T. M., Kresse, T. M., Al-Rashidy, S., Mckee, S., and Shirley, T., 1998, Tipping the scales in long-term karst research-hydrologic characterization of the Savoy Experimental Watershed, Proc. Arkansas Water Resources Central Annual Research Conference, Fayetteville AR.

Brahana, J.V., Ting, T., 2005, Quantification of hydrologic budget parameters for the Vadose Zone and epikarst in a mantled karst: USGS Karst Interest Group Proceedings, p. 144-152.

Campbell, W.C., El Latif, M.A, Foster, J., 1996, Application of Thermography to Karst Hydrology: Journal of Cave and Karst Studies v. 58, no. 3, p. 163-167.

Dogwiler, T. and Wicks, C., 2006, Thermal Variations in the Hyporheic Zone of a Karst Stream: International Journal of Speleology, v. 35, no. 2, p. 59-66.

Goldscheider, N., and Drew, D., (Eds.) 2007, Methods in Karst Hydrogeology, Taylor & Francis, London, p. 264.

Hubbs, K., 2011, United States Geological Survey: Arkansas Water Science Center, Stream Gauge Data received 11/21/2011.

Jones, W., Culver, D., and Herman, J., 2004, Introduction to Epikarst: Karst Waters Institute Special Publication, v. 9, p. 1-7.

Klimchouk, A., 2004, Towards defining, delimiting and classifying epikarst, its origin, processes and variants of geomorphic evolution: Speleogenesis and Evolution of Karst Aquifers, v. 2, no. 1, p. 1-13.

Krothe, N.C., 2003, Groundwater flow and contaminant transport through the epikarst in two karst drainage systems, USA: Materials and Geoenvironment, v. 50, no. 1, p. 177-180.

Luhmann, A., Covington, M., Peters, A., Alexander, S., Anger, C., Green, J., Runkel, A., and E. Alexander, 2009, Classification of Thermal Patterns at Karst Springs and Cave Streams. Ground Water 49, no. 3, p. 324-335 doi: 10.1111/j.1745-6584.2010.00737.x (Figure 3).

National Weather Service, 2011, WFO Monthly/Daily Climate Data Drake Field Fayetteville, AR. Volume 2011 March-August: Fayetteville Arkansas, National Weather Service.

Onset, 2012, HOBO® Data Loggers: http://www.onsetcomp.com/data-logger?gclid=CPi3uMWUsq4CFbAEQAodD1U4Qg (accessed December 2011).

Padilla, A., Pulido-Bosch, A., and Mangin, A., 1994, Relative Importance of Baseflow and Quickflow from Hydrographs of Karst Spring: Journal of Ground Water, v. 32, no. 2, p. 267-276.

Pennington, D., 2010, Karst Drainage-Basin Analysis Using Hydrograph Decomposition Techniques at the Savoy Experimental Watershed, Savoy, Arkansas [M.S. Thesis] 235 p.

Phelan, T., 2002, Public Datasets Integrated with GIS and 3-D Visualization Help Expand Subsurface Conceptual Model: Journal of Cave and Karst Studies, v. 64, no. 1, p.77-81.

Sauer, T.J., Logsdon, S.D., Brahana, J.V., and Murdoch, J.V., 2005, Variation in infiltration with landscape position: Implications for forest productivity and surface water quality: Forest Ecology and Management, v. 220, no. 1-3, p. 118-127, doi:10.1016/j.foreco.2005.08.009.

Ting, T., 2005, Assessing bacterial transport, storage, and viability in mantled karst of northwest Arkansas using clay and scherichia coli labeled with lanthanide series metals, [Ph. D Dissertation] 279 p.

United States Geological Survey, 2010, Seamless Data Warehouse: http://seamless.usgs.gov/ (accessed November 2011).

United States Environmental Protection Agency (EPA), 1988, Application of Dye-Tracing Techniques for Determining Solute-Transport Characteristics of Ground Water in Karst Terranes: Region 4.

White, W., and White, E., 2005, Ground water flux distribution between matrix, fractures, and conduits: constraints on modeling: Speleogenesis and Evolution of Karst Aquifers, v. 3, no. 2, p. 1-6.

White, W., 1999, Conceptual Models for Karstic Aquifers: in Palmer, A.N., Palmer, M.V., and Sasowsky, I.D. eds., Karst Modeling, Special Publication 9: Charles Town, WV, Karst Waters Institute, p.11-16.

Yuan, D., Wu, Y., Li, L., and Jiang, Y., 2008: Modeling Hydrological Responses of Karst Spring to Storm Events: Environmental Geology, v. 55, no. 7, p. 1545-1553.